Provably Physical-Constraint-Preserving Discontinuous Galerkin Methods for Multidimensional Relativistic MHD Equations

Kailiang Wu* and Chi-Wang Shu†

February 15, 2021

Abstract

We propose and analyze a class of robust, uniformly high-order accurate discontinuous Galerkin (DG) schemes for multidimensional relativistic magnetohydrodynamics (RMHD) on general meshes. A distinct feature of the schemes is their physical-constraint-preserving (PCP) property, i.e., they are proven to preserve the subluminal constraint on the fluid velocity and the positivity of density, pressure, and internal energy. This is the first time that provably PCP high-order schemes are achieved for multidimensional RMHD. Developing PCP high-order schemes for RMHD is highly desirable but remains a challenging task, especially in the multidimensional cases, due to the inherent strong nonlinearity in the constraints and the effect of the magnetic divergence-free condition. Inspired by some crucial observations at the PDE level, we construct the provably PCP schemes by using the locally divergence-free DG schemes of the recently proposed symmetrizable RMHD equations as the base schemes, a limiting technique to enforce the PCP property of the DG solutions, and the strong-stability-preserving methods for time discretization. We rigorously prove the PCP property by using a novel "quasi-linearization" approach to handle the highly nonlinear physical constraints, technical splitting to offset the influence of divergence error, and sophisticated estimates to analyze the beneficial effect of the additional source term in the symmetrizable RMHD system. Several two-dimensional numerical examples are provided to further confirm the PCP property and to demonstrate the accuracy, effectiveness and robustness of the proposed PCP schemes.

Keywords: relativistic magnetohydrodynamics, discontinuous Galerkin method, physical-constraint-preserving, high-order accuracy, locally divergence-free

***Mathematics Subject Classification*:** 65M60, 65M12, 35L65, 76W05

*Department of Mathematics, Southern University of Science and Technology, Shenzhen, Guangdong Province 518055, P.R. China. (wukl@sustech.edu.cn).

†Division of Applied Mathematics, Brown University, Providence, RI 02912, USA (Chi-Wang_Shu@brown.edu). Research of C.-W. Shu is supported in part by NSF grants DMS-1719410 and DMS-2010107, and AFOSR grant FA9550-20-1-0055.

1 Introduction

In this paper, we explore robust and high-order accurate numerical schemes for solving relativistic magnetohydrodynamics (RMHD) equations, which are widely used for the description of the dynamics of electrically conducting fluids moving close to the speed of light in the presence of the magnetic field. The RMHD equations play an important role in many fields, such as astrophysics and high energy physics, and have been used to investigate a number of astrophysical scenarios from stellar to galactic scales, e.g., gamma-ray bursts, formation of black holes, astrophysical jets, blast waves of supernova explosions, gravitational collapse and accretion, etc.

The special RMHD equations are often formulated as a nonlinear system of hyperbolic conservation laws

$$\mathbf{U}_t + \nabla \cdot \mathbf{F}(\mathbf{U}) = \mathbf{0}, \tag{1}$$

where $\nabla\cdot = \sum_{i=1}^{d} \frac{\partial}{\partial x_i}$ is the divergence operator with $d \in \{1, 2, 3\}$ denoting the spatial dimensionality. Here the geometrized unit system is used so that the speed of light $c = 1$. In (1), the conservative vector $\mathbf{U} = (D, \mathbf{m}, \mathbf{B}, E)^\top$, and the flux $\mathbf{F} = (\mathbf{F}_1, \ldots, \mathbf{F}_d)$ is defined by

$$\mathbf{F}_i(\mathbf{U}) = \big(Dv_i, v_i\mathbf{m} - B_i\big(W^{-2}\mathbf{B} + (\mathbf{v}\cdot\mathbf{B})\mathbf{v}\big) + p_{tot}\mathbf{e}_i, v_i\mathbf{B} - B_i\mathbf{v}, m_i\big)^\top,$$

with the mass density $D = \rho W$, the momentum vector $\mathbf{m} = (\rho H W^2 + |\mathbf{B}|^2)\mathbf{v} - (\mathbf{v}\cdot\mathbf{B})\mathbf{B}$, the magnetic field $\mathbf{B} = (B_1, B_2, B_3)$, the energy $E = \rho H W^2 - p_{tot} + |\mathbf{B}|^2$, and the vector $\mathbf{e}_i$ being the i-th row of the unit matrix of size 3. In addition, ρ denotes the rest-mass density, $\mathbf{v} = (v_1, v_2, v_3)$ is the velocity field of the fluid, $W = 1/\sqrt{1 - |\mathbf{v}|^2}$ denotes the Lorentz factor, $H = 1 + e + \frac{p}{\rho}$ stands for the specific enthalpy with e being the specific internal energy. p_{tot} represents the total pressure consisting of the thermal pressure p and the magnetic pressure $p_m := \frac{1}{2}\left(W^{-2}|\mathbf{B}|^2 + (\mathbf{v}\cdot\mathbf{B})^2\right)$. In order to close the system (1) an equation of state (EOS) is needed. A general EOS can be expressed as

$$H = H(p, \rho). \tag{2}$$

A simple widely-used one is the ideal EOS

$$H = 1 + \frac{\Gamma p}{(\Gamma - 1)\rho}, \tag{3}$$

with a constant $\Gamma \in (1, 2]$ denoting the adiabatic index, for which the restriction $\Gamma \le 2$ is required by the compressibility assumptions and the relativistic causality [45]. Given a specific EOS, the conservative vector $\mathbf{U}$ and the flux $\mathbf{F}$ can be explicitly expressed by the primitive variables $\{\rho, p, \mathbf{v}, \mathbf{B}\}$. However, unlike the non-relativistic case, there are no explicit formulas for either the flux $\mathbf{F}$ or the primitive variables $\{\rho, \mathbf{v}, p\}$ in terms of $\mathbf{U}$, due to the appearance of the Lorentz factor and other relativistic effects.

The magnetic field should also satisfy an additional divergence-free condition

$$\nabla \cdot \mathbf{B} := \sum_{i=1}^{d} \frac{\partial B_i}{\partial x_i} = 0, \tag{4}$$

which reflects the fact that there are no magnetic monopoles and also appears in the non-relativistic ideal MHD system. In fact, if the initial magnetic field is divergence-free, then the exact solution of the equations (1) always maintains zero divergence. In the design of numerical RMHD schemes, the divergence-free condition (4) should be also accommodated carefully, which causes challenges in addition to the standard difficulties in solving the nonlinear hyperbolic systems. It is widely realized that the condition (4) is important for robust computations, since large divergence error in the magnetic field may cause nonphysical structures or numerical instabilities, see, for example, [12, 3, 37, 22]. In the one-dimensional case ($d = 1$), B_1 is constant so that the condition (4) can be easily enforced in numerical computations. However, in the multidimensional cases ($d \geq 2$), numerical preservation of (4) is indeed nontrivial, and various techniques have been proposed to reduce the divergence error or numerically enforce the condition (4) in some discrete sense; see e.g., [12, 29, 37, 9, 1, 7, 36, 22, 23, 27, 50, 13, 4] and the references therein.

In physics, the density, internal energy and thermal pressure are positive, and the fluid velocity must be slower than the speed of light in the vacuum $c = 1$. In other words, the physically admissible conservative variables $\mathbf{U}$ must stay in the following set

$$\mathcal{G} := \left\{ \mathbf{U} = (D, \mathbf{m}, \mathbf{B}, E)^\top : \ \rho(\mathbf{U}) > 0, \ p(\mathbf{U}) > 0, \ e(\mathbf{U}) > 0, \ |\mathbf{v}(\mathbf{U})| < 1 \right\}, \tag{5}$$

where the functions $\rho(\mathbf{U})$, $p(\mathbf{U})$, $e(\mathbf{U})$ and $\mathbf{v}(\mathbf{U})$ are highly nonlinear and cannot be explicitly formulated in terms of $\mathbf{U}$, due to the relativistic effect. The satisfaction of the constraints (5) is not only necessary for the physical nature of the solution, but also highly desirable and crucial for the robustness of numerical computations. In fact, when any physical constraints in (5) are violated numerically, the discrete problem would become ill-posed because the hyperbolicity is lost, and numerical instability can develop so as to cause the blowup of the numerical solutions and the termination of the simulation. In the past several decades, various numerical schemes were developed for the RMHD, e.g., [20, 10, 26, 38, 17, 51, 2, 57]. However, none of them were rigorously proven to preserve all these constraints, even though they have been applied to successfully simulate some RMHD flows. In fact, most of the existing RMHD schemes do not always maintain these constraints, and thus may suffer from a risk of failure when simulating RMHD problems with large Lorentz factor, low density or pressure, or strong discontinuity. It is therefore highly significant and desirable to develop physical-constraint-preserving (PCP) numerical methods[1] that always keep the solutions in the admissible state set $\mathcal{G}$.

During the past decade, significant progress has been made for constructing bound-preserving high-order accurate schemes for solving hyperbolic partial differential equations, with the aid of two types of limiters. One is a simple scaling limiter for the solution polynomials reconstructed in finite volume methods or evolved by discontinuous Galerkin (DG) methods; see, e.g., [53, 54, 52, 42, 43, 58]. Another one is a flux-correction limiter, see, e.g., [49, 18, 24, 5].

[1] The PCP property defined in this paper refers only to the preservation of the subluminal constraint on fluid velocity and the positivity of density, pressure, and internal energy. Our PCP definition does *not* include the divergence-free constraint (4). The numerical schemes proposed in this paper only maintain a *locally* divergence-free property for the magnetic field.

For more developments, we refer interested readers to the survey [33] and references therein. With these limiting approaches, several PCP methods were developed for the special relativistic hydrodynamics (RHD) without the magnetic field, including high-order accurate PCP finite difference schemes [45], PCP DG schemes [30], PCP central DG schemes [47], and PCP Lagrangian finite volume schemes [25]. It is nontrivial to extend the PCP methods from special to general RHD. An earlier effort [32] was made in this direction but only enforced the positivity of density. Recently, frameworks were established in [39] for designing provably PCP high-order accurate finite volume, finite difference and DG methods for the general RHD. All of the aforementioned PCP methods were restricted to the RHD without the magnetic field $\mathbf{B}$.

Yet, it is still a highly challenging task to seek the provably PCP numerical schemes for the RMHD, mainly due to the effect of the numerical divergence error of $\mathbf{B}$, the intrinsically complicated coupling of the RMHD equations, and the highly nonlinear physical constraints in (5). As mentioned above, there are no explicit expressions of the highly nonlinear functions $\rho(\mathbf{U})$, $p(\mathbf{U})$, $e(\mathbf{U})$ and $\mathbf{v}(\mathbf{U})$ for the RMHD. Taking the ideal EOS case (3) as example, in order to obtain the values of $\{\rho, \mathbf{v}, e, p\}$ from a given vector $\mathbf{U} = (D, \mathbf{m}, \mathbf{B}, E)^\top$, one needs to solve a nonlinear algebraic equation [26]:

$$\theta + |\mathbf{B}|^2 - E + \frac{\Gamma - 1}{\Gamma}\left(\frac{D}{\Upsilon_{\mathbf{U}}(\theta)} - \frac{\theta}{\Upsilon^2_{\mathbf{U}}(\theta)}\right) - \frac{1}{2}\left(\frac{(\mathbf{m}\cdot\mathbf{B})^2}{\theta^2} + \frac{|\mathbf{B}|^2}{\Upsilon^2_{\mathbf{U}}(\theta)}\right) = 0, \tag{6}$$

for the unknown $\theta \in (0, +\infty)$. Here the function $\Upsilon_{\mathbf{U}}(\theta)$ is defined by

$$\Upsilon_{\mathbf{U}}(\theta) = \left(\frac{\theta^2(\theta + |\mathbf{B}|^2)^2 - \left[\theta^2|\mathbf{m}|^2 + (2\theta + |\mathbf{B}|^2)(\mathbf{m}\cdot\mathbf{B})^2\right]}{\theta^2(\theta + |\mathbf{B}|^2)^2}\right)^{-1/2}.$$

Assume that an admissible solution of the equation (6) exists for the given state $\mathbf{U}$, and denote it by $\hat{\theta} = \hat{\theta}(\mathbf{U})$, then we can compute the primitive variables in (5) by

$$\begin{aligned} &\mathbf{v}(\mathbf{U}) = \Big(\mathbf{m} + \hat{\theta}^{-1}(\mathbf{m}\cdot\mathbf{B})\mathbf{B}\Big)/(\hat{\theta} + |\mathbf{B}|^2), && \rho(\mathbf{U}) = \frac{D}{\Upsilon_{\mathbf{U}}(\hat{\theta})}, \\ &p(\mathbf{U}) = \frac{\Gamma - 1}{\Gamma\Upsilon^2_{\mathbf{U}}(\hat{\theta})}\Big(\hat{\theta} - D\Upsilon_{\mathbf{U}}(\hat{\theta})\Big), && e(\mathbf{U}) = \frac{p(\mathbf{U})}{(\Gamma - 1)\rho(\mathbf{U})}. \end{aligned} \tag{7}$$

As clearly shown in the above procedure, checking the admissibility of a given state $\mathbf{U}$ is already a very difficult task. On the other hand, in most of the numerical RMHD schemes, the evolution of the conservative quantities $\{D, \mathbf{m}, \mathbf{B}, E\}$ are generally based on their own conservation laws in (1), while the discrete evolution equations are seemingly not directly related to the constraints in (5) and do not necessarily ensure the desired bounds of the computed primitive variables $\{\rho, p, e, \mathbf{v}\}$. In theory, it is quite difficult to prejudge whether a numerical RMHD scheme is always PCP under all circumstances or not. The study of PCP schemes for the RMHD has remained blank until the recent work in [46], where several important mathematical properties of the set $\mathcal{G}$ were first derived, and PCP schemes were developed for the conservative RMHD equations (1) in *one space dimension*. Moreover, for the multidimensional

conservative RMHD equations, the theoretical analysis in [46] revealed that the PCP property of standard DG and finite volume methods is closely connected with a *discrete divergence-free condition* on the numerical magnetic field. This finding was further extended on general meshes in [48] and was also observed in the non-relativistic ideal MHD case [40]. Moreover, it was shown in [46, 48] that the *multidimensional* first-order Lax-Friedrichs scheme for (1) is generally not PCP, if that discrete version of divergence-free condition is violated slightly. Unfortunately, the required discrete divergence-free condition relies on certain combination of the numerical solution information on adjacent cells, so that it could not be naturally enforced by any existing divergence-free techniques that also work in conjunction with the standard local scaling PCP limiter [46]. Therefore, the design of multidimensional PCP schemes for the RMHD has challenges essentially different from the one-dimensional case. As a result, provably PCP high-order schemes have *not* yet been obtained for the conservative RMHD system (1) in the *multidimensional* cases.

The focus of this paper is to develop a class of provably PCP high-order DG schemes for the multidimensional RMHD with a general EOS on general meshes. This will be the first time that provably PCP high-order schemes are obtained for multidimensional RMHD. Towards achieving this goal, we will make the following efforts in this paper:

1. First, we investigate the PCP property of the exact solutions of the conservative RMHD system (1) at the PDE level. We observe that, if the condition (4) is violated slightly, then the set $\mathcal{G}$ is generally no longer an invariant region for the exact solution of (1), i.e., even the exact solution may fail to be PCP. This is consistent with our previous finding in the non-relativistic ideal MHD case [42]. Therefore, before seeking provably PCP numerical schemes, our first task is to reformulate the RMHD equations so as to accommodate the PCP property at the PDE level. We consider a symmetrizable formulation of the RMHD equations, which we recently proposed in [44], by building the condition (4) into the equations via adding a source term. We show that, for the exact smooth solutions of the new RMHD equations, the PCP property always holds even if $\mathbf{B}$ is *not* divergence-free.

2. Based on the symmetrizable formulation, we construct provably PCP high-order accurate DG schemes on general meshes for the multidimensional RMHD equipped with a general EOS. The key is to properly discretize the symmetrizable RMHD equations so as to eliminate the influence of the numerical divergence error on the PCP property of the resulting DG schemes. We adopt the locally divergence-free DG elements, which enforce zero divergence within each cell, and a suitable discretization of the symmetrization source term, which brings some crucial discrete divergence terms into our schemes and exactly offsets the influence of the divergence error on the PCP property.

3. One key innovation in this paper is the rigorous proof of the PCP property of the proposed high-order accurate DG schemes for the multidimensional RMHD, without requiring any discrete divergence-free condition. There are two main technical challenges in the proof. One is how to explicitly and analytically verify the admissibility of any given conservative

state $\mathbf{U}$, without solving the nonlinear equation (6). This difficulty has been addressed in [46] based on two equivalent forms of the admissible state set $\mathcal{G}$. The other is how to take the advantages of the locally divergence-free property of the numerical magnetic field and our suitable discretization of the source term in the symmetrizable RMHD formulation, to eliminate the influence of the divergence error on the PCP property. Due to the divergence-involving source term and the locally divergence-free DG solutions, the limiting values of the numerical solution on the boundaries of each mesh cell are coupled intrinsically, leading to some standard analysis techniques ([54]) inapplicable in our case. We will overcome this difficulty by using a novel "quasi-linearization" approach to handle the highly nonlinear constraints in (5), technical splitting to offset the influence of divergence error, and sophisticated estimates to analyze the beneficial effect of the symmetrization source term.

4. We implement the proposed PCP DG schemes on two-dimensional Cartesian meshes and demonstrate their accuracy, effectiveness and robustness for several numerical examples. We will show that our PCP schemes, without any artificial treatments, are able to successfully simulate several challenging problems, including a strongly magnetized bast problem with extremely low plasma-beta (2.5×10^{-10}) and two highly supersonic RMHD jets, which are very demanding test cases and their successful simulations were rarely reported in the literature.

The study in this paper is also motivated by our recent work [42, 43] on exploring the positivity-preserving DG methods for the non-relativistic ideal MHD. Compared to the non-relativistic case, the present study is much more challenging, due to the highly nonlinear coupling of the RMHD equations and the complicated mapping from the conservative to primitive variables. Additional technical challenges also arise from the suitable discretization of the symmetrization source term and especially some novel estimate techniques have to be developed to analyze its beneficial effect on the PCP property.

This paper is organized as follows. In Section 2, we introduce some auxiliary observations on the PCP property at the PDE level. In Section 3, some key techniques for the PCP analysis are presented. We discuss the construction and the provably PCP property of our DG schemes in Section 4, and conduct the numerical tests in Section 5. Section 6 concludes the paper.

2 Auxiliary observations on the PCP property at the PDE level

This section introduces our observations on the PCP property for the strong solutions of the conservative formulation (1) and a symmetrizable formulation of the RMHD equations, respectively, with the ideal EOS (3). The findings will provide some insights that guide us to successfully construct the PCP schemes for the RMHD.

We observe that, if $\nabla\cdot\mathbf{B}\neq 0$, then the set $\mathcal{G}$ is generally no longer an invariant region for the exact solution of (1) because $p<0$ may appear. Let us consider the following initial data

$$\begin{aligned}&\rho(\boldsymbol{x},0)=1,\quad \mathbf{v}(\boldsymbol{x},0)=(0.01,\ 0.01,\ 0.01),\quad p(\boldsymbol{x},0)=1-\mathrm{e}^{-\frac{1}{2}|\boldsymbol{x}|^4},\\&\mathbf{B}(\boldsymbol{x},0)=(2,2,2)+\epsilon(\arctan x_1,\ \ \arctan x_2,\ \ \arctan x_3),\end{aligned}\tag{8}$$

where $\boldsymbol{x}=(x_1,\ldots,x_d)$, and $0<\epsilon\ll 1$ indicates a very small nonzero divergence in the magnetic field. Notice that the initial solution (8) is infinitely differentiable and bounded. We then study the Cauchy problem of (1) with (8), by assuming that the exact solution of this problem exists and is smooth for the time t belonging to a small interval $[0,t_*)$, $0<t^*\ll 1$. Since $|\mathbf{v}(\mathbf{0},0)|-1=-0.97<0$ and $\rho(\mathbf{0},0)=1>0$, by the sign-preserving property for continuous functions, there exists a neighborhood Ω of $\mathbf{0}$ in $\mathbb{R}^d$ and $t_0\in(0,,t_*)$ such that $\rho(\boldsymbol{x},t)>0$ and $|\mathbf{v}(\boldsymbol{x},t)|-1<0$, $\forall(\boldsymbol{x},t)\in\Omega\times[0,t_0)$. We now compute the initial temporal derivative of $p\rho^{-\Gamma}$ at $(\boldsymbol{x},t)=(\mathbf{0},0)$. It can be derived from the equations (1) that

$$\frac{\partial}{\partial t}\left(p\rho^{-\Gamma}\right)+\mathbf{v}\cdot\nabla\left(p\rho^{-\Gamma}\right)+(\Gamma-1)\rho^{-\Gamma}(\mathbf{v}\cdot\mathbf{B})\nabla\cdot\mathbf{B}=0.\tag{9}$$

At $(\boldsymbol{x},t)=(\mathbf{0},0)$, we have $\nabla\left(p\rho^{-\Gamma}\right)=\mathbf{0}$ and $\nabla\cdot\mathbf{B}=d\epsilon>0$, which imply $\frac{\partial\left(p\rho^{-\Gamma}\right)}{\partial t}(\mathbf{0},0)=-0.06d(\Gamma-1)\epsilon<0$. Besides, one can observe that $p\rho^{-\Gamma}(\mathbf{0},0)=0$. Thus there exists $t_1\in[0,t_0)$ such that $p\rho^{-\Gamma}(\mathbf{0},t)<0,\ \forall t\in(0,t_1)$. Because $\rho(\boldsymbol{x},t)>0,\ \forall(\boldsymbol{x},t)\in\Omega\times[0,t_0)$, we have $p(\mathbf{0},t)<0,\ \forall t\in(0,t_1)$.

The above analysis infers that if the condition (4) is violated slightly, $\mathcal{G}$ is no longer an invariant region for the exact solution of the equations (1), i.e., the exact solution may fail to be PCP. This observation, along with the results in [46] at the numerical level, demonstrate the unity of continuous and discrete objects, and clearly reveal the intrinsic connection between the PCP property and divergence-free condition.

We remark that (8) is merely a mathematical example and indeed has no practical relevance, because of a vanishing pressure at the origin and the nonzero divergence of the magnetic field. Nevertheless, such a nonphysical situation may appear in numerical solutions — the local pressure can be very close to zero and the magnetic field can be not divergence-free. According to the analysis above, when the condition (4) is violated numerically at $t=t_n$, *even an exact PDE solver* (suppose we have) of the equations (1) for the subsequent simulation ($t>t_n$) may also fail to be PCP. Unfortunately, in most of the multidimensional RMHD schemes including the standard DG methods, the numerical divergence error is generally unavoidable. Although a few globally divergence-free numerical techniques were proposed (see e.g. [23, 27, 50, 13, 4]), the standard local scaling limiter (cf. [54, 46]) for bound preservation can *destroy the globally divergence-free property*. It is therefore difficult to find a numerical technique which can enforce the globally divergence-free property and meet the PCP requirement at the same time.

In order to address the above issue, we propose to consider a symmetrizable formulation of the RMHD equations [44]

$$\mathbf{U}_t+\nabla\cdot\mathbf{F}(\mathbf{U})=-\mathbf{S}(\mathbf{U})\nabla\cdot\mathbf{B},\tag{10}$$

where

$$\mathbf{S}(\mathbf{U}) := \big(0,\ (1-|\mathbf{v}|^2)\mathbf{B} + (\mathbf{v}\cdot\mathbf{B})\mathbf{v},\ \mathbf{v},\ \mathbf{v}\cdot\mathbf{B}\big)^\top. \tag{11}$$

The system (10) is analogous to the Godunov–Powell system [14, 28] for the non-relativistic ideal MHD. It is first proposed in [44] recently for the entropy symmetrization of the RMHD equations. For convenience, we refer to the additional term at the right-hand-size of (10) as "symmetrization source term". Under the condition (4), this source term vanishes, so that the two formulations (10) and (1) are equivalent at the continuous level. However, the inclusion of this source term changes some characters of the equations. As a result, the modified RMHD system (10) becomes symmetrizable, admits a convex thermodynamic entropy pair, and plays a key role in designing entropy stable schemes [44]. These beneficial properties do not hold for the conservative RMHD system (1).

For the PCP point of view, we discover another beneficial property of the symmetrizable RMHD system (10). Specifically, we observe that, at the PDE level, the strong solutions of the symmetrizable equations (10) always maintain the PCP property, even if $\mathbf{B}$ is not divergence-free. Let us study the Cauchy problem of the equations (10), for $\boldsymbol{x} \in \mathbb{R}^d$ and $t > 0$, with the initial condition

$$(\rho, \mathbf{v}, \mathbf{B}, p)(\boldsymbol{x}, 0) = (\rho_0, \mathbf{v}_0, p_0, \mathbf{B}_0)(\boldsymbol{x}), \tag{12}$$

where the magnetic field is *not necessarily divergence-free*. Then we can prove the following result by the method of characteristics.

Proposition 2.1. *Assume the initial data (12) are in $C^1(\mathbb{R}^d)$ with $\rho_0(\boldsymbol{x}) > 0$, $p_0(\boldsymbol{x}) > 0$, and $|\mathbf{v}_0(\boldsymbol{x})| < 1$, $\forall \boldsymbol{x} \in \mathbb{R}^d$. If the Cauchy problem of (10) with (12) has a C^1 solution $(\rho, \mathbf{v}, \mathbf{B}, p)(\boldsymbol{x}, t)$ for $\boldsymbol{x} \in \mathbb{R}^d$ and $0 \le t \le T$, then*

$$\rho(\boldsymbol{x}, t) > 0,\ |\mathbf{v}(\boldsymbol{x}, t)| < 1,\ p(\boldsymbol{x}, t) > 0,\ e(\boldsymbol{x}, t) > 0, \quad \forall \boldsymbol{x} \in \mathbb{R}^d,\ \forall t \in [0, T].$$

In addition, if assuming the solution is C^2, then it holds

$$\min_{\boldsymbol{x}\in\mathbb{R}^d} \frac{\nabla\cdot\mathbf{B}}{\rho W}(\boldsymbol{x}, 0) \le \frac{\nabla\cdot\mathbf{B}}{\rho W}(\boldsymbol{x}, t) \le \max_{\boldsymbol{x}\in\mathbb{R}^d} \frac{\nabla\cdot\mathbf{B}}{\rho W}(\boldsymbol{x}, 0), \qquad \forall t \in [0, T], \tag{13}$$

which implies that the "relative" divergence $\|\rho^{-1}W^{-1}\nabla\cdot\mathbf{B}(\cdot, t)\|_{L^\infty}$ does not grow with t.

Proof. The proof is straightforward and is given in Appendix A for completeness. ∎

As we have already seen, the inclusion of the source term $\mathbf{S}(\mathbf{U})\nabla\cdot\mathbf{B}$ in the symmetrizable RMHD system (10) helps eliminate the effect of nonzero divergence on the PCP property at the PDE level. Now, it is very natural to ask: *For the PCP property at the numerical level, can we get a similar benefit from the system (10)? Can we also eliminate the effect of divergence error to achieve PCP schemes by proper discretization of the new equations (10)?* These questions will be answered by the efforts in the subsequent sections, for which some important analysis techniques are required.

Remark 2.1. *Analogous to the Powell source term for the non-relativistic ideal MHD system [29, 42, 43], the source term in the symmetrizable RMHD system (10) is non-conservative, but is necessary to accommodate the PCP property at the PDE level when the condition (4) is not exactly satisfied. Therefore, in order to achieve the PCP property at the discrete level, our schemes in this paper will be constructed using the symmetrizable formulation (10), which poses additional technical challenges in discretizing the source term properly to ensure its compatibility with the PCP property. As mentioned in [42, 43] on the non-relativistic MHD, there is a conflict between the PCP property which requires the non-conservative source term, and the conservation property which is lost due to the source term. The loss of conservation property leaves the possibility that it may lead to incorrect resolutions for some discontinuous problems, which will be investigated carefully in a separate study. It would be also interesting to explore PCP high-order schemes via the conservative formulation (1) and with an exactly divergence-free numerical technique that can work in conjunction with a bound-preserving limiter.*

Remark 2.2. *For smooth solutions, if the divergence-free condition (4) is met, then equation (9), derived from the conservative system (1), reduces to*

$$S_t + \mathbf{v} \cdot \nabla S = 0 \tag{14}$$

with $S := p\rho^{-\Gamma}$ being the specific entropy. This equation can also be directly derived from the symmetrizable RMHD system (10), without using the divergence-free condition (4). See (60) in the proof of Proposition 2.1. The equation (14) actually describes an entropy transport which "drives" the positivity of p and e, given that $\rho > 0$. For non-smooth solutions, this equation is replaced with the entropy inequality $(\rho S)_t + \nabla \cdot (\mathbf{v}\rho S) \geq 0$, which implies Tadmor's minimum entropy principle [35]: $S(\boldsymbol{x}, t) \geq \min_{\boldsymbol{x}} S(\boldsymbol{x}, 0)$. Several high-order schemes satisfying this principle were developed, e.g., for the (non-relativistic) Euler equations [55, 16, 19] and recently for the RHD equations [41] without magnetic field.

3 Numerical analysis techniques

In this section, we will introduce several important properties of $\mathcal{G}$ and derive some technical estimates, which will be useful in the PCP analysis of the proposed numerical schemes.

3.1 Properties of admissible states

Throughout the rest of this paper, we consider a general causal EOS (2) satisfying

$$\begin{cases} \text{The function } H(p,\rho) \text{ in (2) is differentiable in } \mathbb{R}^+ \times \mathbb{R}^+, \\ H(p,\rho) \geq \sqrt{1 + p^2/\rho^2} + p/\rho, & \forall p, \rho > 0, \\ H(p,\rho)\left(\frac{1}{\rho} - \frac{\partial H(p,\rho)}{\partial p}\right) < \frac{\partial H(p,\rho)}{\partial \rho} < 0, & \forall p, \rho > 0, \end{cases} \tag{15}$$

where the second condition is revealed by the relativistic kinetic theory, and the third condition can be derived from the relativistic causality and assuming that the coefficient of the thermal expansion of the fluids is positive [47]. These assumptions are reasonable because they are valid for most compressible fluids, e.g., the gases. One can verify that the conditions in (15) hold for the ideal EOS (3) and some other commonly used EOSs; see [47].

In order to overcome the challenges arising from the lack of explicit formulas of the functions in (5), the following two equivalent forms of $\mathcal{G}$ were rigorously derived in [46] for the ideal EOS (3) and in [48] for a general EOS (2) satisfying (15).

Lemma 3.1 (First equivalent form). *The set $\mathcal{G}$ define in (5) is **equivalent** to the set*

$$\mathcal{G}_1 := \left\{\mathbf{U} = (D, \mathbf{m}, \mathbf{B}, E)^\top : \ D > 0, \ q(\mathbf{U}) > 0, \ \Psi(\mathbf{U}) > 0\right\},$$

where $q(\mathbf{U}) := E - \sqrt{D^2 + |\mathbf{m}|^2}$ and

$$\Psi(\mathbf{U}) := \big(\Phi(\mathbf{U}) - 2(|\mathbf{B}|^2 - E)\big)\sqrt{\Phi(\mathbf{U}) + |\mathbf{B}|^2 - E} - \sqrt{\frac{27}{2}\Big(D^2|\mathbf{B}|^2 + (\mathbf{m}\cdot\mathbf{B})^2\Big)},$$

with $\Phi(\mathbf{U}) := \sqrt{(|\mathbf{B}|^2 - E)^2 + 3(E^2 - D^2 - |\mathbf{m}|^2)}$.

Lemma 3.2 (Second equivalent form). *The set $\mathcal{G}$ or $\mathcal{G}_1$ is **equivalent** to the set*

$$\mathcal{G}_2 := \left\{\mathbf{U} = (D, \mathbf{m}, \mathbf{B}, E)^\top : \ D > 0, \ \mathbf{U}\cdot\boldsymbol{\xi}^* + p_m^* > 0, \forall \mathbf{B}^* \in \mathbb{R}^3, \forall \mathbf{v}^* \in \mathbb{B}_1(\mathbf{0})\right\},$$

where $\mathbb{B}_1(\mathbf{0}) := \{\boldsymbol{x} \in \mathbb{R}^3 : |\boldsymbol{x}| < 1\}$ denotes the open unit ball centered at $\mathbf{0}$ in $\mathbb{R}^3$, and

$$\boldsymbol{\xi}^* = \left(-\sqrt{1 - |\mathbf{v}^*|^2}, \ -\mathbf{v}^*, \ -(1 - |\mathbf{v}^*|^2)\mathbf{B}^* - (\mathbf{v}^*\cdot\mathbf{B}^*)\mathbf{v}^*, \ 1\right)^\top, \tag{16}$$

$$p_m^* = \frac{(1 - |\mathbf{v}^*|^2)|\mathbf{B}^*|^2 + (\mathbf{v}^*\cdot\mathbf{B}^*)^2}{2}. \tag{17}$$

Remark 3.1. *The auxiliary variables $\mathbf{B}^*$ and $\mathbf{v}^*$ are "free parameters" mathematically. Specifically, in Lemma 3.2 we require that $\mathbf{U}\cdot\boldsymbol{\xi}^* + p_m^* > 0$ holds for **any** $\mathbf{B}^* \in \mathbb{R}^3$ and **any** $\mathbf{v}^* \in \mathbb{B}_1(\mathbf{0})$, where $\boldsymbol{\xi}^*$ and p_m^* are functions of these auxiliary variables as defined in (16)–(17). Geometrically, $\mathbf{B}^*$ and $\mathbf{v}^*$ represent the corresponding magnetic field and velocity of the states on the boundary ($\Psi(\mathbf{U}) = 0$) of the domain $\mathcal{G}$ in the space $\mathbb{R}^8$; see [46] for some details.*

Remark 3.2. *Note that all the constraints in the above two equivalent forms are **explicit** with respect to $\mathbf{U}$. This is a very helpful feature. The first equivalent form $\mathcal{G}_1$ is particularly useful for checking the admissibility of a given state $\mathbf{U}$ and constructing the limiter for developing PCP high-order accurate RMHD schemes. Moreover, the two constraints in the second equivalent form $\mathcal{G}_2$, are both **linear** with respect to $\mathbf{U}$, although two (additional) auxiliary variables $\mathbf{B}^*$ and $\mathbf{v}^*$ are introduced. Such linearity makes $\mathcal{G}_2$ quite suitable for analytically verifying the PCP property of RMHD schemes. It will provide a novel quasi-linearization approach to handle nonlinear physical constraints and is a key to our analysis techniques, which are significantly different from the standard bound-preserving analysis techniques (cf. [54]).*

It is proven in [46] that the admissible state set is convex.

Lemma 3.3. *The admissible state set $\mathcal{G}_1$ is convex.*

3.2 Technical estimates

In order to handle the effect of the source term in the symmetrizable RMHD system (10) on the PCP property of numerical schemes, we derive the following inequality (18), whose discovery is highly nontrivial.

Lemma 3.4. *For any $\mathbf{U} \in \mathcal{G}$, any $\mathbf{B}^* \in \mathbb{R}^3$ and any $\mathbf{v}^* \in \mathbb{B}_1(\mathbf{0})$, it holds*

$$|\mathbf{S}(\mathbf{U}) \cdot \boldsymbol{\xi}^* + \mathbf{v}^* \cdot \mathbf{B}^*| \le \frac{1}{\sqrt{\rho H}} \left(\mathbf{U} \cdot \boldsymbol{\xi}^* + p_m^*\right), \tag{18}$$

where ρ and $H = 1 + e + \frac{p}{\rho}$ are the density and specific enthalpy corresponding to $\mathbf{U}$; and $\boldsymbol{\xi}^*$ and p_m^* are functions of $(\mathbf{v}^*, \mathbf{B}^*)$ as defined in (16) and (17), respectively.

Proof. Notice that, due to the relativistic effect, the function $\mathbf{S}(\mathbf{U})$, defined by $\mathbf{v}$ and $\mathbf{B}$ in (11), also cannot be explicitly formulated in terms of $\mathbf{U}$. Therefore, we have to work on the primitive variables $\{\rho, \mathbf{v}, p, \mathbf{B}\}$ of $\mathbf{U}$, which satisfy $\rho > 0$, $|\mathbf{v}| < 1$ and $p > 0$ because $\mathbf{U} \in \mathcal{G}$.

We observe that

$$\mathbf{S}(\mathbf{U}) \cdot \boldsymbol{\xi}^* + \mathbf{v}^* \cdot \mathbf{B}^* = (\mathbf{v} - \mathbf{v}^*) \cdot \Big((1 - |\mathbf{v}|^2)\mathbf{B} + (\mathbf{v} \cdot \mathbf{B})\mathbf{v} - (1 - |\mathbf{v}^*|^2)\mathbf{B}^* - (\mathbf{v}^* \cdot \mathbf{B}^*)\mathbf{v}^*\Big).$$

Let $\Pi_1 := \mathbf{U} \cdot \boldsymbol{\xi}^* + p_m^*$ and

$$\Pi_2 := \sqrt{\rho H}(\mathbf{v} - \mathbf{v}^*) \cdot \Big((1 - |\mathbf{v}|^2)\mathbf{B} + (\mathbf{v} \cdot \mathbf{B})\mathbf{v} - (1 - |\mathbf{v}^*|^2)\mathbf{B}^* - (\mathbf{v}^* \cdot \mathbf{B}^*)\mathbf{v}^*\Big).$$

Then, we need to prove

$$\Pi_1 \ge |\Pi_2|. \tag{19}$$

We reformulate Π_1 and decompose it into two parts as follows:

$$\begin{aligned}
\Pi_1 &= \rho H W^2 (1 - \mathbf{v} \cdot \mathbf{v}^*) - p - \rho W \sqrt{1 - |\mathbf{v}^*|^2} \\
&\quad + \Big((1 - |\mathbf{v}^*|^2)\mathbf{B}^* + (\mathbf{v}^* \cdot \mathbf{B}^*)\mathbf{v}^*\Big) \cdot (-\mathbf{B}) + \Big(|\mathbf{B}|^2 \mathbf{v} - (\mathbf{v} \cdot \mathbf{B})\mathbf{B}\Big) \cdot (-\mathbf{v}^*) \\
&\quad + \frac{(1 + |\mathbf{v}|^2)|\mathbf{B}|^2 - (\mathbf{v} \cdot \mathbf{B})^2}{2} + \frac{(1 - |\mathbf{v}^*|^2)|\mathbf{B}^*|^2 + (\mathbf{v}^* \cdot \mathbf{B}^*)^2}{2} \\
&= \left[\rho H W^2 (1 - \mathbf{v} \cdot \mathbf{v}^*) - p - \rho W \sqrt{1 - |\mathbf{v}^*|^2}\right] \\
&\quad + \left[\frac{(1 - |\mathbf{v}^*|^2)|\mathbf{B} - \mathbf{B}^*|^2}{2} + \frac{(\mathbf{v}^* \cdot (\mathbf{B} - \mathbf{B}^*))^2}{2} + \frac{|\mathbf{v} - \mathbf{v}^*|^2 |\mathbf{B}|^2}{2} - \frac{((\mathbf{v} - \mathbf{v}^*) \cdot \mathbf{B})^2}{2}\right] \\
&=: \Pi_1^{(1)} + \Pi_1^{(2)}.
\end{aligned}$$

According to the second condition in (15), the first part $\Pi_1^{(1)}$ satisfies

$$\begin{aligned}
\frac{\Pi_1^{(1)}}{\rho H} &= W^2 (1 - \mathbf{v} \cdot \mathbf{v}^*) - \frac{p}{\rho H} - \frac{1}{H} W \sqrt{1 - |\mathbf{v}^*|^2} \ge W^2 (1 - \mathbf{v} \cdot \mathbf{v}^*) - \frac{\frac{H^2 - 1}{2H}\rho}{\rho H} - \frac{1}{H} W \sqrt{1 - |\mathbf{v}^*|^2} \\
&= \frac{1}{2}\left(\frac{1}{H} - W\sqrt{1 - |\mathbf{v}^*|^2}\right)^2 + W^2 (1 - \mathbf{v} \cdot \mathbf{v}^*) - \frac{1}{2} - \frac{W^2 (1 - |\mathbf{v}^*|^2)}{2} \\
&\ge W^2 (1 - \mathbf{v} \cdot \mathbf{v}^*) - \frac{1}{2} - \frac{W^2 (1 - |\mathbf{v}^*|^2)}{2} = \frac{1}{2} W^2 |\mathbf{v} - \mathbf{v}^*|^2.
\end{aligned}$$

It follows that

$$\Pi_1 \geq \frac{1}{2}\rho H W^2 |\mathbf{v}-\mathbf{v}^*|^2 + \Pi_1^{(2)} := \Pi_3.$$

Therefore, in order to prove (18) or (19), it suffices to show

$$\Pi_3 \geq |\Pi_2|.$$

Let us introduce the vector $\mathbf{Z} = (\mathbf{B}^*, \mathbf{B}, \sqrt{\rho H})^\top \in \mathbb{R}^7$. We observe that both Π_3 and Π_2 can be formulated into quadratic forms in the variables $\mathbf{Z}$. ***This highly nontrivial observation is a key of our proof.*** Specifically, we discover that

$$\Pi_3 = \frac{1}{2}\mathbf{Z}^\top \mathbf{A}_3 \mathbf{Z}, \qquad \Pi_2 = \frac{1}{2}\mathbf{Z}^\top \mathbf{A}_2 \mathbf{Z}$$

with

$$\mathbf{A}_3 = \begin{pmatrix} \mathbf{G} & -\mathbf{G} & \mathbf{0}^\top \\ -\mathbf{G} & \mathbf{H} & \mathbf{0}^\top \\ \mathbf{0} & \mathbf{0} & W^2|\mathbf{v}-\mathbf{v}^*|^2 \end{pmatrix}, \qquad \mathbf{A}_2 = \begin{pmatrix} \mathbf{O} & \mathbf{O} & \mathbf{b}_1^\top \\ \mathbf{O} & \mathbf{O} & \mathbf{b}_2^\top \\ \mathbf{b}_1 & \mathbf{b}_2 & 0 \end{pmatrix},$$

where $\mathbf{0} = (0,0,0)$, $\mathbf{O}$ is 3×3 zero matrix, and (note that $\mathbf{v}$ and $\mathbf{v}^*$ are row vectors)

$$\begin{aligned}
\mathbf{G} &= (1-|\mathbf{v}^*|^2)\mathbf{I}_3 + (\mathbf{v}^*)^\top \mathbf{v}^*, \\
\mathbf{H} &= \big(1+|\mathbf{v}-\mathbf{v}^*|^2 - |\mathbf{v}^*|^2\big)\mathbf{I}_3 + (\mathbf{v}^*)^\top \mathbf{v}^* - (\mathbf{v}-\mathbf{v}^*)^\top(\mathbf{v}-\mathbf{v}^*), \\
\mathbf{b}_1 &= (1-|\mathbf{v}^*|^2)(\mathbf{v}^*-\mathbf{v}) + (|\mathbf{v}^*|^2 - \mathbf{v}\cdot\mathbf{v}^*)\mathbf{v}^*, \\
\mathbf{b}_2 &= (1-|\mathbf{v}|^2)(\mathbf{v}-\mathbf{v}^*) + (|\mathbf{v}|^2 - \mathbf{v}\cdot\mathbf{v}^*)\mathbf{v}.
\end{aligned}$$

Then, it suffices to show that both $\mathbf{A}_3+\mathbf{A}_2$ and $\mathbf{A}_3-\mathbf{A}_2$ are positive semi-definite.

Note that $\mathbf{G}$ is symmetric, and its eigenvalues are given by $\{1-|\mathbf{v}^*|^2, 1-|\mathbf{v}^*|^2, 1\}$. Because all of its eigenvalues are positive, the matrix $\mathbf{G}$ is positive definite. Define a nonsingular matrix

$$\mathbf{P}_1 = \begin{pmatrix} \mathbf{I}_3 & \mathbf{O} & \mathbf{0}^\top \\ \mathbf{I}_3 & \mathbf{I}_3 & \mathbf{0}^\top \\ -\mathbf{b}_1\mathbf{G}^{-1} & \mathbf{0} & 1 \end{pmatrix},$$

where $-\mathbf{b}_1\mathbf{G}^{-1} = \mathbf{v}-\mathbf{v}^*$. Then

$$\mathbf{P}_1(\mathbf{A}_3+\mathbf{A}_2)\mathbf{P}_1^\top = \begin{pmatrix} \mathbf{G} & \mathbf{O} & \mathbf{0}^\top \\ \mathbf{O} & \mathbf{H}-\mathbf{G} & \mathbf{b}_1^\top + \mathbf{b}_2^\top \\ \mathbf{0} & \mathbf{b}_1+\mathbf{b}_2 & W^2|\mathbf{v}-\mathbf{v}^*|^2 - \mathbf{b}_1\mathbf{G}^{-1}\mathbf{b}_1^\top \end{pmatrix}, \tag{20}$$

where

$$\mathbf{b}_1+\mathbf{b}_2 = (|\mathbf{v}|^2 - \mathbf{v}\cdot\mathbf{v}^*)\mathbf{v}^* + (|\mathbf{v}^*|^2 - \mathbf{v}\cdot\mathbf{v}^*)\mathbf{v},$$

and the matrix $\mathbf{H}-\mathbf{G}$ is symmetric and given by

$$\mathbf{H}-\mathbf{G} = |\mathbf{v}-\mathbf{v}^*|^2\mathbf{I}_3 - (\mathbf{v}-\mathbf{v}^*)^\top(\mathbf{v}-\mathbf{v}^*).$$

The eigenvalues of $\mathbf{H}-\mathbf{G}$ are $\{0, |\mathbf{v}-\mathbf{v}^*|^2, |\mathbf{v}-\mathbf{v}^*|^2\}$, which are all nonnegative, implying that $\mathbf{H}-\mathbf{G}$ is positive semi-definite.

Now, we would like to show that $\mathbf{P}_1(\mathbf{A}_3+\mathbf{A}_2)\mathbf{P}_1^\top$ is positive semi-definite. Let us first consider two trivial cases:

- If $\mathbf{v}=\mathbf{v}^*$, then $\mathbf{P}_1(\mathbf{A}_3+\mathbf{A}_2)\mathbf{P}_1^\top=\mathbf{O}$, which is positive semi-definite.
- If $\mathbf{v}=\mathbf{0}$, then $\mathbf{b}_1=\mathbf{v}^*=-\mathbf{b}_2$ and $W^2|\mathbf{v}-\mathbf{v}^*|^2-\mathbf{b}_1\mathbf{G}^{-1}\mathbf{b}_1^\top=0$. In this case, $\mathbf{P}_1(\mathbf{A}_3+\mathbf{A}_2)\mathbf{P}_1^\top=\mathrm{diag}\{\mathbf{G},\mathbf{H}-\mathbf{G},0\}$, which is positive semi-definite.

In the following, we shall focus on the nontrivial case that $\mathbf{v}\neq\mathbf{v}^*$ and $\mathbf{v}\neq\mathbf{0}$. For any $\varepsilon>0$, we define

$$\mathbf{Q}_\varepsilon=\begin{pmatrix}\mathbf{H}-\mathbf{G}+\varepsilon\mathbf{I}_3 & \mathbf{b}_1^\top+\mathbf{b}_2^\top\\ \mathbf{b}_1+\mathbf{b}_2 & W^2|\mathbf{v}-\mathbf{v}^*|^2-\mathbf{b}_1\mathbf{G}^{-1}\mathbf{b}_1^\top\end{pmatrix}.$$

Some algebraic manipulations yield that

$$\det(\mathbf{Q}_\varepsilon)=\frac{\varepsilon}{1-|\mathbf{v}|^2}(\varepsilon+|\mathbf{v}-\mathbf{v}^*|^2)\Big(\varepsilon\Pi_4+|\mathbf{v}|^2|\mathbf{v}-\mathbf{v}^*|^4\Big),$$

where

$$\Pi_4:=(1-|\mathbf{v}|^2)\Big((v_1v_2^*-v_2v_1^*)^2+(v_2v_3^*-v_3v_2^*)^2+(v_3v_1^*-v_1v_3^*)^2\Big)+|\mathbf{v}|^2|\mathbf{v}-\mathbf{v}^*|^2.$$

It is evident that $\Pi_4\geq|\mathbf{v}|^2|\mathbf{v}-\mathbf{v}^*|^2$. For any $\varepsilon>0$, the matrix $\mathbf{H}-\mathbf{G}+\varepsilon\mathbf{I}_3$ is positive definite, and when $\mathbf{v}\neq\mathbf{v}^*$ and $\mathbf{v}\neq\mathbf{0}$, it holds

$$\det(\mathbf{Q}_\varepsilon)\geq\frac{\varepsilon}{1-|\mathbf{v}|^2}(\varepsilon+|\mathbf{v}-\mathbf{v}^*|^2)|\mathbf{v}-\mathbf{v}^*|^2|\mathbf{v}|^2\Big(\varepsilon+|\mathbf{v}-\mathbf{v}^*|^2\Big)>0.$$

This implies that the leading principal minors of $\mathbf{Q}_\varepsilon$ are all positive, and thus $\mathbf{Q}_\varepsilon$ is positive definite for any $\varepsilon>0$, $\mathbf{v}\neq\mathbf{v}^*$ and $\mathbf{v}\neq\mathbf{0}$. Taking the limit $\varepsilon\to0$, we obtain that $\mathbf{Q}_0$ is positive semi-definite, which further yields that $\mathbf{P}_1(\mathbf{A}_3+\mathbf{A}_2)\mathbf{P}_1^\top=\mathrm{diag}\{\mathbf{G},\mathbf{Q}_0\}$ is positive semi-definite, for the nontrivial case ($\mathbf{v}\neq\mathbf{v}^*$ and $\mathbf{v}\neq\mathbf{0}$). In conclusion, for all the cases, $\mathbf{P}_1(\mathbf{A}_3+\mathbf{A}_2)\mathbf{P}_1^\top$ is positive semi-definite.

Because $\mathbf{A}_3+\mathbf{A}_2$ and $\mathbf{P}_1(\mathbf{A}_3+\mathbf{A}_2)\mathbf{P}_1^\top$ are congruent, $\mathbf{A}_3+\mathbf{A}_2$ is positive semi-definite. Similar arguments imply that $\mathbf{A}_3-\mathbf{A}_2$ is also positive semi-definite. Hence

$$\Pi_3\pm\Pi_2=\frac{1}{2}\mathbf{Z}^\top(\mathbf{A}_3\pm\mathbf{A}_2)\mathbf{Z}\geq0,$$

which yields $\Pi_1\geq\Pi_3\geq|\Pi_2|$. The proof is complete. ■

We will also need the following technical inequality (21), which was derived in [46], to handle the effect of the flux in numerical PCP analysis.

Lemma 3.5. *If $\mathbf{U}\in\mathcal{G}$, then for any $\lambda\in[-1,1]$, any $\mathbf{B}^*\in\mathbb{R}^3$ and any $\mathbf{v}^*\in\mathbb{B}_1(\mathbf{0})$, it holds*

$$\big(\mathbf{U}+\lambda\mathbf{F}_i(\mathbf{U})\big)\cdot\boldsymbol{\xi}^*+p_m^*\geq-\lambda\big(v_i^*p_m^*-B_i(\mathbf{v}^*\cdot\mathbf{B}^*)\big),\tag{21}$$

where $i\in\{1,2,\cdots,d\}$, and $\boldsymbol{\xi}^*$ and p_m^* are defined in (16) and (17), respectively.

For any vector $\mathbf{n}=(n_1,\cdots,n_d)\in\mathbb{R}^d$, we introduce the following inner product notations

$$\langle\mathbf{n},\mathbf{v}\rangle:=\sum_{k=1}^d n_kv_k,\qquad\langle\mathbf{n},\mathbf{B}\rangle:=\sum_{k=1}^d n_kB_k,\qquad\langle\mathbf{n},\mathbf{F}\rangle:=\sum_{k=1}^d n_k\mathbf{F}_k,\tag{22}$$

which will be frequently used in this paper. Then we can generalize Lemma 3.5.

Lemma 3.6. *If $\mathbf{U} \in \mathcal{G}$, then for any $\lambda \in [-1,1]$, any $\mathbf{B}^* \in \mathbb{R}^3$, any $\mathbf{v}^* \in \mathbb{B}_1(\mathbf{0})$, and any unit vector $\mathbf{n} \in \mathbb{R}^d$, one has*

$$\big(\mathbf{U} + \lambda\big\langle \mathbf{n}, \mathbf{F}(\mathbf{U})\big\rangle\big) \cdot \boldsymbol{\xi}^* + p_m^* \geq -\lambda\big(\langle \mathbf{n}, \mathbf{v}^*\rangle p_m^* - \langle \mathbf{n}, \mathbf{B}\rangle(\mathbf{v}^* \cdot \mathbf{B}^*)\big). \tag{23}$$

Proof. Let $\mathbf{Q}_\mathbf{n} \in \mathbb{R}^{3\times 3}$ be a rotational matrix associated with the unit vector $\mathbf{n}$ and satisfying

$$\mathbf{e}_1 \mathbf{Q}_\mathbf{n} = (\mathbf{n}, \mathbf{0}_{3-d}), \tag{24}$$

where $\mathbf{e}_1 = (1,0,0)$, and $\mathbf{0}_{3-d}$ denotes the zero vector in $\mathbb{R}^{3-d}$. The rotational invariance of the RMHD system implies

$$\big\langle \mathbf{n}, \mathbf{F}(\mathbf{U})\big\rangle = \mathbf{Q}^{-1}\mathbf{F}_1(\mathbf{Q}\mathbf{U}), \tag{25}$$

where $\mathbf{Q} = \mathrm{diag}\{1, \mathbf{Q}_\mathbf{n}, \mathbf{Q}_\mathbf{n}, 1\}$. As a rotational matrix, $\mathbf{Q}_\mathbf{n}$ is orthogonal. Define $\widehat{\mathbf{B}}^* := \mathbf{B}^*\mathbf{Q}_\mathbf{n}^\top$ and $\widehat{\mathbf{v}}^* := \mathbf{v}^*\mathbf{Q}_\mathbf{n}^\top$, then one can verify that $\widehat{\mathbf{v}}^* \in \mathbb{B}_1(\mathbf{0})$ and

$$\widehat{\mathbf{v}}^* \cdot \widehat{\mathbf{B}}^* = \mathbf{v}^* \cdot \mathbf{B}^*, \qquad \widehat{p}_m^* := \frac{(1-|\widehat{\mathbf{v}}^*|^2)|\widehat{\mathbf{B}}^*|^2 + (\widehat{\mathbf{v}}^* \cdot \widehat{\mathbf{B}}^*)^2}{2} = p_m^*, \tag{26}$$

$$\widehat{\boldsymbol{\xi}}^* = \left(-\sqrt{1-|\widehat{\mathbf{v}}^*|^2},\ -\widehat{\mathbf{v}}^*,\ -(1-|\widehat{\mathbf{v}}^*|^2)\widehat{\mathbf{B}}^* - (\widehat{\mathbf{v}}^* \cdot \widehat{\mathbf{B}}^*)\widehat{\mathbf{v}}^*,\ 1\right)^\top = \mathbf{Q}\boldsymbol{\xi}^*. \tag{27}$$

For $\mathbf{U} \in \mathcal{G}$, using the first equivalent form in Lemma 3.1 we obtain $\widehat{\mathbf{U}} := \mathbf{Q}\mathbf{U} \in \mathcal{G}_1 = \mathcal{G}$. Let $\widehat{\mathbf{B}}$ be the magnetic field corresponding to $\widehat{\mathbf{U}}$. It satisfies $\widehat{\mathbf{B}} = \mathbf{B}\mathbf{Q}_\mathbf{n}^\top$. Let $\widehat{v}_1^*$ and $\widehat{B}_1$ denote the first components of $\widehat{\mathbf{v}}^*$ and $\widehat{\mathbf{B}}$, respectively. Then, we have

$$\widehat{v}_1^* = \mathbf{e}_1 \cdot \mathbf{v}^* = \mathbf{e}_1 \cdot (\mathbf{v}^*\mathbf{Q}_\mathbf{n}^\top) = (\mathbf{e}_1\mathbf{Q}_\mathbf{n}) \cdot \mathbf{v}^* = \langle \mathbf{n}, \mathbf{v}^*\rangle, \qquad \widehat{B}_1 = \langle \mathbf{n}, \mathbf{B}\rangle, \tag{28}$$

where equation (24) has been used. Lemma 3.5 for $\widehat{\mathbf{U}} \in \mathcal{G}$, $\widehat{\mathbf{B}}^* \in \mathbb{R}^3$ and $\widehat{\mathbf{v}}^* \in \mathbb{B}_1(\mathbf{0})$ implies

$$\begin{aligned}
0 &\leq \big(\widehat{\mathbf{U}} + \lambda\mathbf{F}_1(\widehat{\mathbf{U}})\big) \cdot \widehat{\boldsymbol{\xi}}^* + \widehat{p}_m^* + \lambda\big(\widehat{v}_1^*\widehat{p}_m^* - \widehat{B}_1(\widehat{\mathbf{v}}^* \cdot \widehat{\mathbf{B}}^*)\big) \\
&= \big(\mathbf{Q}\mathbf{U} + \lambda\mathbf{F}_1(\mathbf{Q}\mathbf{U})\big) \cdot \big(\mathbf{Q}\boldsymbol{\xi}^*\big) + p_m^* + \lambda\big(\langle \mathbf{n}, \mathbf{v}^*\rangle p_m^* - \langle \mathbf{n}, \mathbf{B}\rangle(\mathbf{v}^* \cdot \mathbf{B}^*)\big) \\
&= \big(\mathbf{U} + \lambda\big\langle \mathbf{n}, \mathbf{F}(\mathbf{U})\big\rangle\big) \cdot \boldsymbol{\xi}^* + p_m^* + \lambda\big(\langle \mathbf{n}, \mathbf{v}^*\rangle p_m^* - \langle \mathbf{n}, \mathbf{B}\rangle(\mathbf{v}^* \cdot \mathbf{B}^*)\big),
\end{aligned}$$

where we have used the equations (26)–(28) in the first equality, and the equation (25) and the orthogonality of $\mathbf{Q}$ in the second equality. The proof is complete. ∎

4 Provably PCP DG Schemes

In this section, we construct PCP high-order DG schemes for the multidimensional RMHD based on the symmetrizable form (10). For the purpose of clarity, we will mainly focus on the spatially 2D case ($d = 2$). Our PCP methods and theoretical analyses can be extended to the spatially 3D case ($d = 3$).

Assume that the physical domain Ω in the 2D space is discretized by a mesh $\mathcal{T}_h$. In general, the mesh may be unstructured and consists of polygonal cells. We also partition the time interval into a mesh $\{t_0 = 0, t_{n+1} = t_n + \Delta t_n, 0 \leq n < N_t\}$, where Δt_n denotes the time step-size and will be determined by some suitable CFL condition. In this section, we will frequently use the capital letter K to denote an arbitrary cell in $\mathcal{T}_h$, and the lower-case letter k will always stand for the DG polynomial degree.

4.1 Outline of the PCP schemes

Let $\boldsymbol{x} \in \mathbb{R}^d$ be the spatial coordinate vector. We define the locally divergence-free DG finite element space [7]:

$$\mathbb{W}_h^k = \left\{ \mathbf{u} = (u_1, \cdots, u_8)^\top : \ u_\ell\big|_K \in \mathbb{P}^k(K), \forall \ell, \ \sum_{i=1}^{d} \frac{\partial u_{4+i}}{\partial x_i}\bigg|_K = 0, \ \forall K \in \mathcal{T}_h \right\},$$

where $\mathbb{P}^k(K)$ denotes the space of polynomials, in cell K, of total degree up to k. To define the PCP DG schemes, we also introduce the following two subsets of $\mathbb{W}_h^k$:

$$\overline{\mathbb{G}}_h^k := \left\{ \mathbf{u} \in \mathbb{W}_h^k : \ \frac{1}{|K|}\int_K \mathbf{u}(\boldsymbol{x})\mathrm{d}\boldsymbol{x} \in \mathcal{G}, \ \ \forall K \in \mathcal{T}_h \right\}, \tag{29}$$

$$\mathbb{G}_h^k := \left\{ \mathbf{u} \in \overline{\mathbb{G}}_h^k : \ \mathbf{u}\big|_K(\boldsymbol{x}) \in \mathcal{G}, \ \ \forall \boldsymbol{x} \in \mathbb{S}_K, \ \forall K \in \mathcal{T}_h \right\}, \tag{30}$$

where $|K|$ denotes the area of the cell K, and $\mathbb{S}_K$ denotes the set of some critical points in K which will be specified later.

Definition 4.1. *A DG scheme is defined to be PCP if its solutions always stay in $\mathbb{G}_h^k$. For clarity, if a DG scheme preserves the numerical solutions in $\overline{\mathbb{G}}_h^k$, then we say it satisfies a "weak" PCP property.*

Lemma 4.1. *The sets $\overline{\mathbb{G}}_h^k$ and $\mathbb{G}_h^k$ are both convex. In addition, for any vector function $\mathbf{u} \in [L^2(\Omega)]^8$ satisfying $\mathbf{u}(\boldsymbol{x}) \in \mathcal{G}$, $\forall \boldsymbol{x} \in \Omega$, we have $\mathbf{P}_w(\mathbf{u}) \in \overline{\mathbb{G}}_h^k$, where $\mathbf{P}_w$ denoting the L^2-projection into $\mathbb{W}_h^k$.*

Proof. According to Lemmas 3.1 and 3.3, $\mathcal{G} = \mathcal{G}_1$ is a convex set. For any $\mathbf{u}_1(\boldsymbol{x}), \mathbf{u}_2(\boldsymbol{x}) \in \overline{\mathbb{G}}_h^k$ and any $\lambda \in [0,1]$, we have

$$\frac{1}{|K|}\int_K \big(\lambda\mathbf{u}_1 + (1-\lambda)\mathbf{u}_2\big)\mathrm{d}\boldsymbol{x} = \lambda\left(\frac{1}{|K|}\int_K \mathbf{u}_1\mathrm{d}\boldsymbol{x}\right) + (1-\lambda)\left(\frac{1}{|K|}\int_K \mathbf{u}_2\mathrm{d}\boldsymbol{x}\right) \in \mathcal{G}, \ \ \forall K \in \mathcal{T}_h,$$

which implies $\lambda\mathbf{u}_1 + (1-\lambda)\mathbf{u}_2 \in \overline{\mathbb{G}}_h^k$. Thus $\overline{\mathbb{G}}_h^k$ is a convex set. Similar argument shows that $\mathbb{G}_h^k$ is convex. For any $\mathbf{u}(\boldsymbol{x}) \in [L^2(\Omega)]^8$ satisfying $\mathbf{u}(\boldsymbol{x}) \in \mathcal{G}, \forall \boldsymbol{x} \in \Omega$, we have $\frac{1}{|K|}\int_K \mathbf{P}_w(\mathbf{u})\mathrm{d}\boldsymbol{x} = \frac{1}{|K|}\int_K \mathbf{u}\mathrm{d}\boldsymbol{x}$, which belongs to $\mathcal{G}$ due to the convexity of $\mathcal{G}$. It follows that $\mathbf{P}_w(\mathbf{u}) \in \overline{\mathbb{G}}_h^k$. ∎

We aim at constructing PCP high-order accurate DG schemes that always preserve the DG solution function $\mathbf{U}_h(\boldsymbol{x}, t)$ in the set $\mathbb{G}_h^k$ for all $t \in \{t_n : 0 \le n \le N_t\}$. This goal will be achieved by following three steps:

1. First, we will seek in Section 4.2 a suitable spatial discretization of symmetrizable RMHD system (10), such that the resulting discrete equation, which can be put in ODE form as $\frac{d}{dt}\mathbf{U}_h = \mathbf{L}_h(\mathbf{U}_h)$, satisfies the "weak" PCP property

$$\text{if} \ \ \mathbf{U}_h \in \mathbb{G}_h^k, \qquad \text{then} \ \ \mathbf{U}_h + \Delta t\mathbf{L}_h(\mathbf{U}_h) \in \overline{\mathbb{G}}_h^k, \tag{31}$$

under some CFL condition on Δt. *The property* (31) *is very important. It is extremely nontrivial to find a DG discretization for the RMHD that can be proven to satisfy* (31). Some traditional methods including standard DG schemes for the conservative RMHD equations (1) do not satisfy (31) in general.

2. Then, we further discretize the ODE system $\frac{d}{dt}\mathbf{U}_h = \mathbf{L}_h(\mathbf{U}_h)$ in time using a strong-stability-preserving (SSP) explicit Runge-Kutta method [15].

3. Finally, a local scaling PCP limiting procedure, which will be introduced in Section 4.3, is applied to the intermediate solutions of the Runge-Kutta discretization. This procedure corresponds to an operator $\mathbf{\Pi}_h : \overline{\mathbb{G}}_h^k \longrightarrow \mathbb{G}_h^k$, which maps the numerical solutions from $\overline{\mathbb{G}}_h^k$ to $\mathbb{G}_h^k$ and satisfies

$$\frac{1}{|K|}\int_K \mathbf{\Pi}_h(\mathbf{u})\mathrm{d}\boldsymbol{x} = \frac{1}{|K|}\int_K \mathbf{u}\mathrm{d}\boldsymbol{x}, \qquad \forall K \in \mathcal{T}_h, \quad \forall \mathbf{u} \in \overline{\mathbb{G}}_h^k. \tag{32}$$

The PCP limiter is required only for high-order DG methods with $k \geq 1$; for the first-order DG method ($k = 0$), $\mathbf{\Pi}_h$ becomes the identity operator.

Let $\mathbf{U}_h^n$ denote the numerical solution at time $t = t_n$. The resulting fully discrete PCP DG methods, with a N_r-stage SSP Runge-Kutta method, can be written in the following form:

- Set $\mathbf{U}_h^0 = \mathbf{\Pi}_h \mathbf{P}_w(\mathbf{U}(\boldsymbol{x}, 0))$;
- For $n = 0, \ldots, N_t - 1$, compute $\mathbf{U}_h^{n+1}$ as follows:
  - (i) set $\mathbf{U}_h^{(0)} = \mathbf{U}_h^n$;
  - (ii) for $i = 1, \ldots, N_r$ compute the intermediate solutions:

$$\mathbf{U}_h^{(i)} = \mathbf{\Pi}_h \left\{ \sum_{\ell=0}^{i-1} \left[\alpha_{i\ell} \left(\mathbf{U}_h^{(\ell)} + \beta_{i\ell} \Delta t_n \mathbf{L}_h(\mathbf{U}_h^{(\ell)}) \right) \right] \right\}; \tag{33}$$

  - (iii) set $\mathbf{U}_h^{n+1} = \mathbf{U}_h^{(N_r)}$;

where the SSP Runge-Kutta method has been written into a convex combination of formally forward Euler methods, and the associated parameters $\alpha_{i\ell}$ and $\beta_{i\ell}$ are all non-negative and satisfy $\sum_{\ell=0}^{i-1} \alpha_{i\ell} = 1$. Some SSP Runge-Kutta methods can be found in [15, 34], e.g., a commonly-used three-stage third-order version is given by

$$\begin{aligned} &\alpha_{10} = 1, \quad \alpha_{20} = 3/4, \quad \alpha_{21} = 1/4, \quad \alpha_{30} = 1/3, \quad \alpha_{31} = 0, \quad \alpha_{32} = 2/3, \\ &\beta_{10} = 1, \quad \beta_{20} = 0, \quad \beta_{21} = 1, \quad \beta_{30} = 0, \quad \beta_{31} = 0, \quad \beta_{32} = 1. \end{aligned} \tag{34}$$

Remark 4.1. *At each Runge-Kutta stage, the PCP property of the above fully discrete DG schemes is enforced by the operator* $\mathbf{\Pi}_h$*, which can only act on functions in* $\overline{\mathbb{G}}_h^k$*. That is, we require the convex combination* $\sum_{\ell=0}^{i-1} \left[\alpha_{i\ell}\big(\mathbf{U}_h^{(\ell)} + \beta_{i\ell}\Delta t_n \mathbf{L}_h(\mathbf{U}_h^{(\ell)})\big)\right] \in \overline{\mathbb{G}}_h^k$*, which is guaranteed*

by the weak PCP property (31) and the convexity of $\overline{\mathbb{G}}_h^k$. On the other hand, the PCP limiting operator $\mathbf{\Pi}_h$ enforces $\mathbf{U}_h^{(\ell)} \in \mathbb{G}_h^k$, $0 \le \ell < i$, which, in turn, meets the condition required by the weak PCP property (31) for the next Runge-Kutta stage evolution. Therefore, the weak PCP property (31) and the PCP limiting operator $\mathbf{\Pi}_h$ work in conjunction with each other and become two key ingredients of the proposed PCP schemes.

In what follows, we shall describe in detail the operators $\mathbf{L}_h$ and $\mathbf{\Pi}_h$, and also specify the point set $\mathbb{S}_K$ in the definition (30) of $\mathbb{G}_h^k$. We will prove the weak PCP property (31) of the DG spatial discretization in Theorem 4.1 and the PCP property of the fully discrete DG schemes in Theorems 4.3 and 4.4.

4.2 The operator $\mathbf{L}_h$ and the weak PCP property

We now derive a suitable spatial discretization such that the resulting operator $\mathbf{L}_h$ satisfies the weak PCP property (31). Following our previous work on the non-relativistic ideal MHD [42, 43], we consider a special locally divergence-free DG discretization for the symmetrizable RMHD system (10):

$$\frac{d}{dt}\int_K \mathbf{U}_h(\boldsymbol{x},t)\cdot\mathbf{u}\mathrm{d}\boldsymbol{x} = \int_K \mathbf{F}(\mathbf{U}_h)\cdot\nabla\mathbf{u}\mathrm{d}\boldsymbol{x} - \sum_{\mathscr{E}\in\partial K}\int_{\mathscr{E}} \mathbf{u}^{\mathrm{int}(K)}\cdot\left[\hat{\mathbf{F}}\left(\mathbf{U}_h^{\mathrm{int}(K)},\mathbf{U}_h^{\mathrm{ext}(K)};\mathbf{n}_{\mathscr{E},K}\right) + \frac{1}{2}\left\langle \mathbf{n}_{\mathscr{E},K}, \mathbf{B}_h^{\mathrm{ext}(K)} - \mathbf{B}_h^{\mathrm{int}(K)}\right\rangle \mathbf{S}\big(\mathbf{U}_h^{\mathrm{int}(K)}\big)\right]\mathrm{d}s, \qquad \forall \mathbf{u}\in\mathbb{W}_h^k, \tag{35}$$

where ∂K denotes the boundary of the cell K; $\mathbf{n}_{\mathscr{E},K}$ is the outward unit normal to the edge $\mathscr{E}$ of K; the inner product $\langle\cdot,\cdot\rangle$ is defined in (22); the superscripts "ext(K)" and "int(K)" indicate that the corresponding limits of $\mathbf{U}_h(\boldsymbol{x})$ at the cell edges are taken from the exterior and interior of K, respectively. In (35), $\hat{\mathbf{F}}$ denotes the numerical flux. Our PCP framework is applicable to any suitable numerical flux provided it ensures the "weak" PCP property in (31). In this paper, we take the numerical flux as the global Lax-Friedrichs flux

$$\hat{\mathbf{F}}\left(\mathbf{U}_h^{\mathrm{int}(K)},\mathbf{U}_h^{\mathrm{ext}(K)};\mathbf{n}_{\mathscr{E},K}\right) = \frac{1}{2}\left(\left\langle \mathbf{n}_{\mathscr{E},K}, \mathbf{F}(\mathbf{U}_h^{\mathrm{int}(K)}) + \mathbf{F}(\mathbf{U}_h^{\mathrm{ext}(K)})\right\rangle - a(\mathbf{U}_h^{\mathrm{ext}(K)} - \mathbf{U}_h^{\mathrm{int}(K)})\right), \tag{36}$$

where a denotes the numerical viscosity parameter. We choose a as the speed of light in vacuum $c = 1$, which a simple upper bound of all wave speeds in the theory of special relativity. This choice is merely for ease of conducting rigorous theoretical analysis. By numerical experiments, we observed that the local or global Lax-Friedrichs flux with suitably smaller numerical viscosity should also satisfy the "weak" PCP property, although a rigorous PCP proof in that case is yet not available due to some technical challenges in theory.

The term $\langle \mathbf{n}_{\mathscr{E},K}, \mathbf{B}_h^{\mathrm{ext}(K)} - \mathbf{B}_h^{\mathrm{int}(K)}\rangle \mathbf{S}\big(\mathbf{U}_h^{\mathrm{int}(K)}\big)$ in (35) is derived from a suitable discretization of the source term in the symmetrizable RMHD system (10), with the locally divergence-free property of $\mathbf{B}_h$ being taken into account. This term is proportional to the jump of the normal component of the magnetic field across cell boundaries. Since this jump is zero for the exact

solution, it is very small (at the level of truncation error) for numerical solutions in smooth region. However, the inclusion of this term is crucial for achieving the property (31), as demonstrated by our theoretical analysis later.

Of course, we have to replace the element and boundary integrals in (35) by some quadrature rules with the at least $2k$ algebraic degree of accuracy. For example, we can approximate the boundary integral by the Gauss quadrature with $Q = k + 1$ points:

$$\begin{aligned}
&\int_{\mathscr{E}} \mathbf{u}^{\mathrm{int}(K)} \cdot \left[\hat{\mathbf{F}} \left(\mathbf{U}_h^{\mathrm{int}(K)}, \mathbf{U}_h^{\mathrm{ext}(K)}; \mathbf{n}_{\mathscr{E},K} \right) + \frac{1}{2} \left\langle \mathbf{n}_{\mathscr{E},K}, \mathbf{B}_h^{\mathrm{ext}(K)} - \mathbf{B}_h^{\mathrm{int}(K)} \right\rangle \mathbf{S}\big(\mathbf{U}_h^{\mathrm{int}(K)}\big) \right] \mathrm{d}s \\
&\quad \approx |\mathscr{E}| \sum_{q=1}^{Q} \omega_q \mathbf{u}^{\mathrm{int}(K)}(\boldsymbol{x}_{\mathscr{E}}^{(q)}) \cdot \left[\hat{\mathbf{F}} \left(\mathbf{U}_h^{\mathrm{int}(K)}(\boldsymbol{x}_{\mathscr{E}}^{(q)}, t), \mathbf{U}_h^{\mathrm{ext}(K)}(\boldsymbol{x}_{\mathscr{E}}^{(q)}, t); \mathbf{n}_{\mathscr{E},K} \right) \right. \\
&\qquad \left. + \frac{1}{2} \left\langle \mathbf{n}_{\mathscr{E},K}, \mathbf{B}_h^{\mathrm{ext}(K)}(\boldsymbol{x}_{\mathscr{E}}^{(q)}, t) - \mathbf{B}_h^{\mathrm{int}(K)}(\boldsymbol{x}_{\mathscr{E}}^{(q)}, t) \right\rangle \mathbf{S} \left(\mathbf{U}_h^{\mathrm{int}(K)}(\boldsymbol{x}_{\mathscr{E}}^{(q)}, t) \right) \right],
\end{aligned}$$

where $|\mathscr{E}|$ denotes the length of the edge $\mathscr{E}$, $\{\boldsymbol{x}_{\mathscr{E}}^{(q)}\}_{1\le q\le Q}$ are the quadrature points on $\mathscr{E}$, and $\{\omega_q\}_{1\le q\le Q}$ are the associated weights with $\sum_{q=1}^{Q} \omega_q = 1$. The element integral $\int_K \mathbf{F}(\mathbf{U}_h)\cdot\nabla\mathbf{u} d\boldsymbol{x}$ can also be approximated by some 2D quadrature $|K| \sum_{q=1}^{\breve{Q}} \breve{\omega}_q \mathbf{F}(\mathbf{U}_h(\breve{\boldsymbol{x}}_K^{(q)}, t)) \cdot \nabla\mathbf{u}(\breve{\boldsymbol{x}}_K^{(q)})$, where $\breve{\boldsymbol{x}}_K^{(q)}$ and $\breve{\omega}_q$ denote the quadrature points and weights, respectively.

Finally, we obtain the following weak DG formulation:

$$\frac{d}{dt} \int_K \mathbf{U}_h \cdot \mathbf{u} \mathrm{d}\boldsymbol{x} = \mathcal{J}_K(\mathbf{U}_h, \mathbf{u}), \qquad \forall \mathbf{u} \in \mathbb{W}_h^k, \tag{37}$$

where $\mathcal{J}_K(\mathbf{U}_h, \mathbf{u}) = \sum_{i=1}^{3} \mathcal{J}_K^{(i)}(\mathbf{U}_h, \mathbf{u})$ with

$$\begin{aligned}
\mathcal{J}_K^{(1)} &= -\sum_{\mathscr{E}\in\partial K} \left\{ |\mathscr{E}| \sum_{q=1}^{Q} \omega_q \hat{\mathbf{F}} \left(\mathbf{U}_h^{\mathrm{int}(K)}(\boldsymbol{x}_{\mathscr{E}}^{(q)}), \mathbf{U}_h^{\mathrm{ext}(K)}(\boldsymbol{x}_{\mathscr{E}}^{(q)}); \mathbf{n}_{\mathscr{E},K} \right) \cdot \mathbf{u}^{\mathrm{int}(K)}(\boldsymbol{x}_{\mathscr{E}}^{(q)}) \right\}, \\
\mathcal{J}_K^{(2)} &= -\frac{1}{2} \sum_{\mathscr{E}\in\partial K} \left\{ |\mathscr{E}| \sum_{q=1}^{Q} \omega_q \left\langle \mathbf{n}_{\mathscr{E},K}, \mathbf{B}_h^{\mathrm{ext}(K)}(\boldsymbol{x}_{\mathscr{E}}^{(q)}) - \mathbf{B}_h^{\mathrm{int}(K)}(\boldsymbol{x}_{\mathscr{E}}^{(q)}) \right\rangle \mathbf{S} \left(\mathbf{U}_h^{\mathrm{int}(K)}(\boldsymbol{x}_{\mathscr{E}}^{(q)}) \right) \cdot \mathbf{u}^{\mathrm{int}(K)}(\boldsymbol{x}_{\mathscr{E}}^{(q)}) \right\}, \\
\mathcal{J}_K^{(3)} &= |K| \sum_{q=1}^{\breve{Q}} \breve{\omega}_q \mathbf{F}(\mathbf{U}_h(\breve{\boldsymbol{x}}_K^{(q)})) \cdot \nabla\mathbf{u}(\breve{\boldsymbol{x}}_K^{(q)}),
\end{aligned}$$

and for notational convenience, we suppress the t dependence of all quantities hereafter, unless confusion arises otherwise. As the standard DG methods (cf. [8, 6]), the weak form (37) can be rewritten in the ODE form as

$$\frac{d}{dt}\mathbf{U}_h = \mathbf{L}_h(\mathbf{U}_h), \tag{38}$$

after choosing a suitable basis of $\mathbb{W}_h^k$ and representing $\mathbf{U}_h$ as a linear combination of the basis functions; see [8, 6] for details. Note that the cell average of $\mathbf{U}_h$, denoted by $\bar{\mathbf{U}}_K := \frac{1}{|K|}\int_K \mathbf{U}_h d\boldsymbol{x}$, satisfies the following time evolution equation

$$\frac{d}{dt}\bar{\mathbf{U}}_K = \widetilde{\boldsymbol{\mathcal{J}}}_K(\mathbf{U}_h), \qquad \forall K \in \mathcal{T}_h, \tag{39}$$

where $\widetilde{\boldsymbol{\mathcal{J}}}_K(\mathbf{U}_h) = \widetilde{\boldsymbol{\mathcal{J}}}_K^{(1)}(\mathbf{U}_h) + \widetilde{\boldsymbol{\mathcal{J}}}_K^{(2)}(\mathbf{U}_h)$ with

$$\widetilde{\boldsymbol{\mathcal{J}}}_K^{(1)}(\mathbf{U}_h) = -\frac{1}{|K|}\sum_{\mathscr{E}\in\partial K}\left\{|\mathscr{E}|\sum_{q=1}^{Q}\omega_q\hat{\mathbf{F}}\left(\mathbf{U}_h^{\mathrm{int}(K)}(\boldsymbol{x}_{\mathscr{E}}^{(q)}),\mathbf{U}_h^{\mathrm{ext}(K)}(\boldsymbol{x}_{\mathscr{E}}^{(q)});\mathbf{n}_{\mathscr{E},K}\right)\right\},$$

$$\widetilde{\boldsymbol{\mathcal{J}}}_K^{(2)}(\mathbf{U}_h) = -\frac{1}{2|K|}\sum_{\mathscr{E}\in\partial K}\left\{|\mathscr{E}|\sum_{q=1}^{Q}\omega_q\left\langle\mathbf{n}_{\mathscr{E},K},\mathbf{B}_h^{\mathrm{ext}(K)}(\boldsymbol{x}_{\mathscr{E}}^{(q)})-\mathbf{B}_h^{\mathrm{int}(K)}(\boldsymbol{x}_{\mathscr{E}}^{(q)})\right\rangle\mathbf{S}\left(\mathbf{U}_h^{\mathrm{int}(K)}(\boldsymbol{x}_{\mathscr{E}}^{(q)})\right)\right\}.$$

We are now in a position to rigorously prove that the above DG spatial discretization satisfies the weak PCP property (31). To this end, we first need to specify the point set $\mathbb{S}_K$ in the definition (30) of $\mathbb{G}_h^k$. Assume that there exists on each cell $K\in\mathcal{T}_h$ a special 2D quadrature satisfies the following requirements:

(i) The quadrature rule is exact for integrals of all the 2D polynomials of total degree k on the cell K.

(ii) The quadrature weights are all positive.

(iii) The quadrature nodes must include all the Gauss points $\boldsymbol{x}_{\mathscr{E}}^{(q)}$, $1\le q\le Q$, $\forall\mathscr{E}\in\partial K$.

Let $\{\widetilde{\boldsymbol{x}}_K^{(q)}\}_{q=1}^{\widetilde{Q}}$, $\widetilde{Q}\ge 0$, denote the other (possible) quadrature points that exclude all the edge Gauss points $\{\boldsymbol{x}_{\mathscr{E}}^{(q)}\}$. We define the set of all quadrature nodes by

$$\widehat{\mathbb{S}}_K := \{\boldsymbol{x}_{\mathscr{E}}^{(q)}, 1\le q\le Q, \forall\mathscr{E}\in\partial K\}\cup\{\widetilde{\boldsymbol{x}}_K^{(q)}, 1\le q\le\widetilde{Q}\}.$$

According to the above requirement, this special quadrature satisfies

$$\frac{1}{|K|}\int_K u(\boldsymbol{x})\mathrm{d}\boldsymbol{x} = \sum_{\mathscr{E}\in\partial K}\sum_{q=1}^{Q}\varpi_{\mathscr{E}}^{(q)}u(\boldsymbol{x}_{\mathscr{E}}^{(q)})+\sum_{q=1}^{\widetilde{Q}}\widetilde{\varpi}_q u(\widetilde{\boldsymbol{x}}_K^{(q)}),\quad\forall u\in\mathbb{P}^k(K),\tag{40}$$

where $\{\varpi_{\mathscr{E}}^{(q)}\}$ and $\{\widetilde{\varpi}_q\}$ denote the quadrature weights, which are all positive. Such a quadrature was first constructed in [53, 54] on rectangular cells by tensor products of Gauss–Lobatto and Gauss quadratures. It can also be designed on triangular cells and more general polygons, see, e.g., [56, 11]. Notice that we will not use this special quadrature for computing any integrals, but only employ it for the following theoretical PCP analysis and the PCP limiter presented later.

Given this special quadrature, we define the point set $\mathbb{S}_K$ required in (30) as

$$\mathbb{S}_K = \widehat{\mathbb{S}}_K\cup\breve{\mathbb{S}}_K,\tag{41}$$

where $\breve{\mathbb{S}}_K := \{\breve{\boldsymbol{x}}_K^{(q)}, 1\le q\le\breve{Q}\}$ are the quadrature points involved in $\mathcal{J}_K^{(3)}$. The inclusion of $\breve{\mathbb{S}}_K$ means that we require $\mathbf{U}_h(\breve{\boldsymbol{x}}_K^{(q)})\in\mathcal{G}$. This special requirement is not involved in the non-relativistic case; it is used here to ensure the existence and uniqueness of the physically admissible solution of the nonlinear equation (6) and thus to obtain the physical primitive variables from $\mathbf{U}_h(\breve{\boldsymbol{x}}_K^{(q)})$ by (7), so as to successfully compute $\mathbf{F}(\mathbf{U}_h(\breve{\boldsymbol{x}}_K^{(q)}))$ in $\mathcal{J}_K^{(3)}$. Such a

consideration is due to the fact that the flux $\mathbf{F}(\mathbf{U})$ and the source $\mathbf{S}(\mathbf{U})$ cannot be explicitly formulated in terms of $\mathbf{U}$ for the RMHD and thus must be computed using the corresponding primitive variables. Note that the edge quadrature points $\{\boldsymbol{x}_{\mathscr{E}}^{(q)}\}$, involved in $\mathcal{J}_K^{(1)}$ and $\mathcal{J}_K^{(2)}$, are already included in $\widehat{\mathbb{S}}_K$.

Based on the point set $\mathbb{S}_K$ defined above, we establish the weak PCP property (31) for the high-order semi-discrete DG scheme (38) as follows.

Theorem 4.1. *Let $\mathbb{G}_K^h$ be the set defined by (30) with $\mathbb{S}_K$ specified in (41). Then, the weak PCP property (31) holds under the following CFL condition on the time step-size Δt:*

$$\Delta t \frac{|\mathscr{E}|}{|K|}\big(a + \sigma_{K,\mathscr{E},q}(\mathbf{U}_h)\big) < \frac{\varpi_{\mathscr{E}}^{(q)}}{\omega_q}, \quad 1 \le q \le Q, \ \forall \mathscr{E} \in \partial K, \ \forall K \in \mathcal{T}_h, \tag{42}$$

where $\sigma_{K,\mathscr{E},q}(\mathbf{U}_h) := \frac{1}{2}\left|\left\langle \mathbf{n}_{\mathscr{E},K}, \mathbf{B}_{\mathscr{E},q}^{\mathrm{int}(K)} - \mathbf{B}_{\mathscr{E},q}^{\mathrm{ext}(K)} \right\rangle\right| / \sqrt{\rho_{\mathscr{E},q}^{\mathrm{int}(K)} H_{\mathscr{E},q}^{\mathrm{int}(K)}}$ with the shortened notations $\mathbf{U}_{\mathscr{E},q}^{\mathrm{int}(K)} := \mathbf{U}_h^{\mathrm{int}(K)}(\boldsymbol{x}_{\mathscr{E}}^{(q)})$ and $\mathbf{U}_{\mathscr{E},q}^{\mathrm{ext}(K)} := \mathbf{U}_h^{\mathrm{ext}(K)}(\boldsymbol{x}_{\mathscr{E}}^{(q)})$.

Proof. In order to prove $\mathbf{U}_h + \Delta t \mathbf{L}_h(\mathbf{U}_h) \in \overline{\mathbb{G}}_h^k$ in (31), it suffices to show

$$\bar{\mathbf{U}}_K^{\Delta t} := \bar{\mathbf{U}}_K + \Delta t \widetilde{\boldsymbol{\mathcal{J}}}_K(\mathbf{U}_h) \in \mathcal{G}, \qquad \forall K \in \mathcal{T}_h, \tag{43}$$

under the CFL condition (42) and the condition that $\mathbf{U}_h \in \mathbb{G}_h^k$. Substituting the formula of the numerical flux (36) into $\widetilde{\boldsymbol{\mathcal{J}}}_K^{(1)}(\mathbf{U}_h)$, we reformulate $\widetilde{\boldsymbol{\mathcal{J}}}_K^{(1)}(\mathbf{U}_h)$ and decompose it into three parts:

$$\begin{aligned}
\widetilde{\boldsymbol{\mathcal{J}}}_K^{(1)}(\mathbf{U}_h) = {} & \frac{a}{2|K|} \sum_{\mathscr{E}\in\partial K} \left[|\mathscr{E}| \sum_{q=1}^{Q} \omega_q \left(\mathbf{U}_{\mathscr{E},q}^{\mathrm{int}(K)} - \frac{1}{a} \left\langle \mathbf{n}_{\mathscr{E},K}, \mathbf{F}\big(\mathbf{U}_{\mathscr{E},q}^{\mathrm{int}(K)}\big) \right\rangle \right) \right] \\
& + \frac{a}{2|K|} \sum_{\mathscr{E}\in\partial K} \left[|\mathscr{E}| \sum_{q=1}^{Q} \omega_q \left(\mathbf{U}_{\mathscr{E},q}^{\mathrm{ext}(K)} - \frac{1}{a} \left\langle \mathbf{n}_{\mathscr{E},K}, \mathbf{F}\big(\mathbf{U}_{\mathscr{E},q}^{\mathrm{ext}(K)}\big) \right\rangle \right) \right] \\
& - \frac{a}{|K|} \sum_{\mathscr{E}\in\partial K} \left(|\mathscr{E}| \sum_{q=1}^{Q} \omega_q \mathbf{U}_{\mathscr{E},q}^{\mathrm{int}(K)} \right) =: \widetilde{\boldsymbol{\mathcal{J}}}_K^{(1,1)} + \widetilde{\boldsymbol{\mathcal{J}}}_K^{(1,2)} + \widetilde{\boldsymbol{\mathcal{J}}}_K^{(1,3)}.
\end{aligned}$$

Then $\bar{\mathbf{U}}_K^{\Delta t}$ can be rewritten as

$$\bar{\mathbf{U}}_K^{\Delta t} = \boldsymbol{\Xi}_1 + \boldsymbol{\Xi}_2 + \boldsymbol{\Xi}_3 + \boldsymbol{\Xi}_4, \tag{44}$$

with $\boldsymbol{\Xi}_i := \Delta t \widetilde{\boldsymbol{\mathcal{J}}}_K^{(1,i)}$, $i = 1, 2$, $\boldsymbol{\Xi}_3 := \bar{\mathbf{U}}_K + \Delta t \widetilde{\boldsymbol{\mathcal{J}}}_K^{(1,3)}$ and

$$\boldsymbol{\Xi}_4 := \Delta t \widetilde{\boldsymbol{\mathcal{J}}}_K^{(2)} = \frac{\Delta t}{2|K|} \sum_{\mathscr{E}\in\partial K} \left[|\mathscr{E}| \sum_{q=1}^{Q} \omega_q \left\langle \mathbf{n}_{\mathscr{E},K}, \mathbf{B}_{\mathscr{E},q}^{\mathrm{int}(K)} - \mathbf{B}_{\mathscr{E},q}^{\mathrm{ext}(K)} \right\rangle \mathbf{S}\left(\mathbf{U}_{\mathscr{E},q}^{\mathrm{int}(K)} \right) \right].$$

Since $\mathcal{G} = \mathcal{G}_2$ as shown in Lemma 3.2, it remains to prove $\bar{\mathbf{U}}_K^{\Delta t} \in \mathcal{G}_2$, $\forall K \in \mathcal{T}_h$.

We first show $\bar{D}_K^{\Delta t} > 0$. Because $\mathbf{U}_h \in \mathbb{G}_h^k$ and $\widehat{\mathbb{S}}_K \subset \mathbb{S}_K$, we have $\mathbf{U}_{\mathscr{E},q}^{\mathrm{int}(K)} \in \mathcal{G}$ and $\mathbf{U}_{\mathscr{E},q}^{\mathrm{ext}(K)} \in \mathcal{G}$ for all $1 \le q \le Q$, $\mathscr{E} \in \partial K$ and $K \in \mathcal{T}_h$. Note that the first component of

$\mathbf{U}_{\mathscr{E},q}^{\mathrm{int}(K)} - \frac{1}{a}\langle \mathbf{n}_{\mathscr{E},K}, \mathbf{F}(\mathbf{U}_{\mathscr{E},q}^{\mathrm{int}(K)})\rangle$ equals $D_{\mathscr{E},q}^{\mathrm{int}(K)}\big(1-\frac{1}{a}\langle \mathbf{n}_{\mathscr{E},K}, \mathbf{v}_{\mathscr{E},q}^{\mathrm{int}(K)}\rangle\big) \geq D_{\mathscr{E},q}^{\mathrm{int}(K)}\big(1-\frac{1}{a}|\mathbf{v}_{\mathscr{E},q}^{\mathrm{int}(K)}|\big) > 0$, which implies that the first component of $\boldsymbol{\Xi}_1$ is positive. Similarly, we know that the first component of $\boldsymbol{\Xi}_2$ is also positive. Notice that the first component of $\boldsymbol{\Xi}_4$ is zero. Therefore, the first component of $\bar{\mathbf{U}}_K^{\Delta t}$ is larger than that of $\boldsymbol{\Xi}_3$. It gives

$$\begin{aligned}
\bar{D}_K^{\Delta t} &> \bar{D}_K - \frac{a\Delta t}{|K|}\sum_{\mathscr{E}\in\partial K}\left(|\mathscr{E}|\sum_{q=1}^{Q}\omega_q D_{\mathscr{E},q}^{\mathrm{int}(K)}\right)\\
&= \sum_{\mathscr{E}\in\partial K}\sum_{q=1}^{Q}\varpi_{\mathscr{E}}^{(q)} D_{\mathscr{E},q}^{\mathrm{int}(K)} + \sum_{q=1}^{\widetilde{Q}}\widetilde{\varpi}_q D_h^{\mathrm{int}(K)}(\widetilde{\boldsymbol{x}}_K^{(q)}) - \frac{a\Delta t}{|K|}\sum_{\mathscr{E}\in\partial K}\left(|\mathscr{E}|\sum_{q=1}^{Q}\omega_q D_{\mathscr{E},q}^{\mathrm{int}(K)}\right)\\
&\geq \sum_{\mathscr{E}\in\partial K}\sum_{q=1}^{Q}\left[\omega_q D_{\mathscr{E},q}^{\mathrm{int}(K)}\left(\frac{\varpi_{\mathscr{E}}^{(q)}}{\omega_q} - a\Delta t\frac{|\mathscr{E}|}{|K|}\right)\right] \geq 0,
\end{aligned}$$

where the equation (40) and the condition (42) have been used.

We then prove that $\bar{\mathbf{U}}_K^{\Delta t}\cdot\boldsymbol{\xi}^* + p_m^* > 0$ for any auxiliary variables $\mathbf{B}^* \in \mathbb{R}^3$ and $\mathbf{v}^* \in \mathbb{B}_1(\mathbf{0})$. It follows from (44) that

$$\bar{\mathbf{U}}_K^{\Delta t}\cdot\boldsymbol{\xi}^* + p_m^* = I_1 + I_2 + I_3 + I_4, \tag{45}$$

with $I_1 := \boldsymbol{\Xi}_1\cdot\boldsymbol{\xi}^* + \eta$, $I_2 := \boldsymbol{\Xi}_1\cdot\boldsymbol{\xi}^* + \eta$, $I_3 := \boldsymbol{\Xi}_3\cdot\boldsymbol{\xi}^* + p_m^* - 2\eta$, $I_4 := \boldsymbol{\Xi}_4\cdot\boldsymbol{\xi}^*$, and

$$\eta := \frac{a\Delta t}{2|K|}\sum_{\mathscr{E}\in\partial K}|\mathscr{E}|p_m^*.$$

Next we estimate suitable lower bounds of I_i for $1\leq i\leq 4$. Using Lemma 3.6 and noting that for polynomials of degree k the Q-point ($Q = k+1$) Gauss quadrature rule is exact, we deduce that

$$\begin{aligned}
I_1 &= \frac{a\Delta t}{2|K|}\sum_{\mathscr{E}\in\partial K}\left\{|\mathscr{E}|\sum_{q=1}^{Q}\omega_q\left[\left(\mathbf{U}_{\mathscr{E},q}^{\mathrm{int}(K)} - \frac{1}{a}\left\langle \mathbf{n}_{\mathscr{E},K}, \mathbf{F}(\mathbf{U}_{\mathscr{E},q}^{\mathrm{int}(K)})\right\rangle\right)\cdot\boldsymbol{\xi}^* + p_m^*\right]\right\}\\
&\geq \frac{a\Delta t}{2|K|}\sum_{\mathscr{E}\in\partial K}\left\{|\mathscr{E}|\sum_{q=1}^{Q}\omega_q\left[\frac{1}{a}\Big(\langle \mathbf{n}_{\mathscr{E},K}, \mathbf{v}^*\rangle\, p_m^* - \left\langle \mathbf{n}_{\mathscr{E},K}, \mathbf{B}_{\mathscr{E},q}^{\mathrm{int}(K)}\right\rangle(\mathbf{v}^*\cdot\mathbf{B}^*)\Big)\right]\right\}\\
&= \frac{\Delta t}{2|K|}\sum_{\mathscr{E}\in\partial K}\left\{|\mathscr{E}|\sum_{q=1}^{Q}\omega_q\Big(-\left\langle \mathbf{n}_{\mathscr{E},K}, \mathbf{B}_{\mathscr{E},q}^{\mathrm{int}(K)}\right\rangle(\mathbf{v}^*\cdot\mathbf{B}^*)\Big)\right\}\\
&= -\frac{\Delta t(\mathbf{v}^*\cdot\mathbf{B}^*)}{2|K|}\sum_{\mathscr{E}\in\partial K}\int_{\mathscr{E}}\left\langle \mathbf{n}_{\mathscr{E},K}, \mathbf{B}_h^{\mathrm{int}(K)}\right\rangle \mathrm{d}s =: -\frac{\Delta t(\mathbf{v}^*\cdot\mathbf{B}^*)}{2|K|}\mathrm{div}_K^{\mathrm{int}}\mathbf{B}_h.
\end{aligned}\tag{46}$$

Similarly, we obtain

$$I_2 \geq -\frac{\Delta t(\mathbf{v}^*\cdot\mathbf{B}^*)}{2|K|}\sum_{\mathscr{E}\in\partial K}\int_{\mathscr{E}}\left\langle \mathbf{n}_{\mathscr{E},K}, \mathbf{B}_h^{\mathrm{ext}(K)}\right\rangle \mathrm{d}s =: -\frac{\Delta t(\mathbf{v}^*\cdot\mathbf{B}^*)}{2|K|}\mathrm{div}_K^{\mathrm{ext}}\mathbf{B}_h. \tag{47}$$

Note that

$$I_3 = \bar{\mathbf{U}}_K\cdot\boldsymbol{\xi}^* + p_m^* - \frac{a\Delta t}{|K|}\sum_{\mathscr{E}\in\partial K}\left(|\mathscr{E}|\sum_{q=1}^{Q}\omega_q\Big(\mathbf{U}_{\mathscr{E},q}^{\mathrm{int}(K)}\cdot\boldsymbol{\xi}^* + p_m^*\Big)\right),$$

and a lower bound of $\bar{\mathbf{U}}_K \cdot \boldsymbol{\xi}^* + p_m^*$ can be derived using (40) as follows:

$$\begin{aligned}\bar{\mathbf{U}}_K \cdot \boldsymbol{\xi}^* + p_m^* &= \sum_{\mathscr{E}\in\partial K}\sum_{q=1}^{Q} \varpi_{\mathscr{E}}^{(q)} \left(\mathbf{U}_{\mathscr{E},q}^{\mathrm{int}(K)} \cdot \boldsymbol{\xi}^* + p_m^*\right) + \sum_{q=1}^{\widetilde{Q}} \widetilde{\varpi}_q \left(\mathbf{U}_h^{\mathrm{int}(K)}(\widetilde{\boldsymbol{x}}_K^{(q)}) \cdot \boldsymbol{\xi}^* + p_m^*\right) \\ &\geq \sum_{\mathscr{E}\in\partial K}\sum_{q=1}^{Q} \varpi_{\mathscr{E}}^{(q)} \left(\mathbf{U}_{\mathscr{E},q}^{\mathrm{int}(K)} \cdot \boldsymbol{\xi}^* + p_m^*\right),\end{aligned}$$

where $\mathbf{U}_h^{\mathrm{int}(K)}(\widetilde{\boldsymbol{x}}_K^{(q)}) \in \mathcal{G} = \mathcal{G}_2$, which implies $\mathbf{U}_h^{\mathrm{int}(K)}(\widetilde{\boldsymbol{x}}_K^{(q)}) \cdot \boldsymbol{\xi}^* + p_m^* > 0$, has been used. It follows that

$$I_3 \geq \sum_{\mathscr{E}\in\partial K}\sum_{q=1}^{Q} \left(\mathbf{U}_{\mathscr{E},q}^{\mathrm{int}(K)} \cdot \boldsymbol{\xi}^* + p_m^*\right) \left(\varpi_{\mathscr{E}}^{(q)} - a\Delta t \omega_q \frac{|\mathscr{E}|}{|K|}\right). \tag{48}$$

Thanks to the inequality (18) constructed in Lemma 3.4, we have

$$\beta(\mathbf{S}(\mathbf{U}) \cdot \boldsymbol{\xi}^*) \geq -\frac{|\beta|}{\sqrt{\rho H}} (\mathbf{U} \cdot \boldsymbol{\xi}^* + p_m^*) - \beta(\mathbf{v}^* \cdot \mathbf{B}^*), \qquad \forall \beta \in \mathbb{R}, \quad \forall \mathbf{U} \in \mathcal{G}.$$

It follows that

$$\begin{aligned}\left\langle \mathbf{n}_{\mathscr{E},K}, \mathbf{B}_{\mathscr{E},q}^{\mathrm{int}(K)} - \mathbf{B}_{\mathscr{E},q}^{\mathrm{ext}(K)} \right\rangle \mathbf{S}\big(\mathbf{U}_{\mathscr{E},q}^{\mathrm{int}(K)}\big) \cdot \boldsymbol{\xi}^* &\geq \left\langle \mathbf{n}_{\mathscr{E},K}, \mathbf{B}_{\mathscr{E},q}^{\mathrm{ext}(K)} - \mathbf{B}_{\mathscr{E},q}^{\mathrm{int}(K)} \right\rangle (\mathbf{v}^* \cdot \mathbf{B}^*) \\ &- \left(\rho_{\mathscr{E},q}^{\mathrm{int}(K)} H_{\mathscr{E},q}^{\mathrm{int}(K)}\right)^{-\frac{1}{2}} \left|\left\langle \mathbf{n}_{\mathscr{E},K}, \mathbf{B}_{\mathscr{E},q}^{\mathrm{int}(K)} - \mathbf{B}_{\mathscr{E},q}^{\mathrm{ext}(K)} \right\rangle\right| \left(\mathbf{U}_{\mathscr{E},q}^{\mathrm{int}(K)} \cdot \boldsymbol{\xi}^* + p_m^*\right).\end{aligned} \tag{49}$$

Let

$$I_5 := -\frac{\Delta t}{|K|} \sum_{\mathscr{E}\in\partial K}\sum_{q=1}^{Q} \omega_q \sigma_{K,\mathscr{E},q} \big(\mathbf{U}_{\mathscr{E},q}^{\mathrm{int}(K)} \cdot \boldsymbol{\xi}^* + p_m^*\big).$$

With the help of (49), we then obtain a lower bound for I_4:

$$\begin{aligned}I_4 &\geq \frac{\Delta t}{2|K|} \sum_{\mathscr{E}\in\partial K} \left[|\mathscr{E}| \sum_{q=1}^{Q} \omega_q \left\langle \mathbf{n}_{\mathscr{E},K}, \mathbf{B}_{\mathscr{E},q}^{\mathrm{ext}(K)} - \mathbf{B}_{\mathscr{E},q}^{\mathrm{int}(K)} \right\rangle (\mathbf{v}^* \cdot \mathbf{B}^*)\right] + I_5 \\ &= \frac{\Delta t (\mathbf{v}^* \cdot \mathbf{B}^*)}{2|K|} \left(\mathrm{div}_K^{\mathrm{ext}} \mathbf{B}_h - \mathrm{div}_K^{\mathrm{int}} \mathbf{B}_h\right) + I_5.\end{aligned} \tag{50}$$

Thanks to the locally divergence-free property of $\mathbf{B}_h(\boldsymbol{x})$, we have

$$\mathrm{div}_K^{\mathrm{int}} \mathbf{B}_h = \sum_{\mathscr{E}\in\partial K} \int_{\mathscr{E}} \left\langle \mathbf{n}_{\mathscr{E},K}, \mathbf{B}_h^{\mathrm{int}(K)} \right\rangle \mathrm{d}s = \int_K \nabla \cdot \mathbf{B}_h^{\mathrm{int}(K)}(\boldsymbol{x}) \mathrm{d}\boldsymbol{x} = 0, \tag{51}$$

where Green's theorem has been used. Combining the estimates (46)–(50) and using (51) and (45), we obtain

$$\begin{aligned}\bar{\mathbf{U}}_K^{\Delta t} \cdot \boldsymbol{\xi}^* + p_m^* &\geq \sum_{\mathscr{E}\in\partial K}\sum_{q=1}^{Q} \left(\mathbf{U}_{\mathscr{E},q}^{\mathrm{int}(K)} \cdot \boldsymbol{\xi}^* + p_m^*\right) \left(\varpi_{\mathscr{E}}^{(q)} - a\Delta t \omega_q \frac{|\mathscr{E}|}{|K|}\right) + I_5 \\ &= \sum_{\mathscr{E}\in\partial K}\sum_{q=1}^{Q} \omega_q \left(\mathbf{U}_{\mathscr{E},q}^{\mathrm{int}(K)} \cdot \boldsymbol{\xi}^* + p_m^*\right) \left[\frac{\varpi_{\mathscr{E}}^{(q)}}{\omega_q} - \Delta t \frac{|\mathscr{E}|}{|K|}(a + \sigma_{K,\mathscr{E},q})\right] > 0,\end{aligned}$$

where the condition (42) has been used in the last inequality. Therefore, we have

$$\bar{\mathbf{U}}_K^{\Delta t} \cdot \boldsymbol{\xi}^* + p_m^* > 0, \qquad \forall \mathbf{B}^* \in \mathbb{R}^3,\ \forall \mathbf{v}^* \in \mathbb{B}_1(\mathbf{0}),$$

which, along with $\bar{D}_K^{\Delta t} > 0$, yield $\bar{\mathbf{U}}_K^{\Delta t} \in \mathcal{G}_2 = \mathcal{G}$. The proof is complete. ■

Remark 4.2. *The quantities* $\mathrm{div}_K^{\mathrm{int}}\mathbf{B}_h$ *and* $\mathrm{div}_K^{\mathrm{ext}}\mathbf{B}_h$*, defined in the lower bounds in* (46) *and* (47) *respectively, denote the discrete divergence. They are also defined in [46] to quantify the influence of the divergence error on the PCP property of the standard DG methods, for which the discrete divergence-free condition* $\mathrm{div}_K^{\mathrm{ext}}\mathbf{B}_h = \mathrm{div}_K^{\mathrm{int}}\mathbf{B}_h = 0$ *is required. However, the present DG schemes are proven to be PCP without requiring that additional condition, thanks to two key technical ingredients. The first is to use a locally divergence-free DG discretization, which leads to zero divergence within each cell, so that the term* $\mathrm{div}_K^{\mathrm{int}}\mathbf{B}_h$ *vanishes. The second is a suitable discretization of the source term in the symmetrizable RMHD system* (10) *which gives* $\mathcal{J}_K^{(2)}(\mathbf{U}_h, \mathbf{u})$ *in* (37)*. It brings some new divergence terms, as shown in the lower bound in* (50)*, which exactly offset the divergence term in* (47)*. As a result, the influence of nonzero divergence error on the PCP property is fully eliminated. This feature is analogous to the continuous case that the inclusion of the source* $\mathbf{S}(\mathbf{U})\nabla\cdot\mathbf{B}$ *in the RMHD equations* (10) *helps eliminate the effect of nonzero divergence* $\nabla\cdot\mathbf{B}$ *on the PCP property at the PDE level. Again, these results demonstrate the unity of discrete and continuous objects.*

For the first-order DG method ($k = 0$), we have $\mathbf{U}_h\big|_K(\boldsymbol{x}) \equiv \bar{\mathbf{U}}_K$ and $\mathbb{G}_h^k = \overline{\mathbb{G}}_h^k$ so that the PCP and weak PCP properties are equivalent in this case, and the PCP property can be proven under a milder CFL condition as shown in Theorem 4.2.

Theorem 4.2. *For the first-order* ($k = 0$) *semi-discrete DG scheme* (38)*, the PCP property* (31) *holds under the following CFL type condition*

$$\Delta t \left(\frac{a}{2|K|} \sum_{\mathscr{E}\in\partial K} |\mathscr{E}| + \frac{|\mathrm{div}_K \mathbf{B}_h|}{\sqrt{\bar{\rho}_K \bar{H}_K}} \right) < 1, \quad \forall K \in \mathcal{T}_h, \tag{52}$$

where $\mathrm{div}_K\mathbf{B}_h$ *denotes a discrete divergence of* $\mathbf{B}_h$ *on the cell* K *defined by*

$$\mathrm{div}_K \mathbf{B}_h := \frac{1}{|K|} \sum_{\mathscr{E}\in\partial K} |\mathscr{E}| \left\langle \mathbf{n}_{\mathscr{E},K}, \frac{\bar{\mathbf{B}}_K + \bar{\mathbf{B}}_{K_{\mathscr{E}}}}{2} \right\rangle, \tag{53}$$

with $K_{\mathscr{E}}$ *denoting the adjacent cell that shares the edge* $\mathscr{E}$ *with the cell* K*. In* (52)–(53)*, the notations* $\bar{\rho}_K$*,* $\bar{H}_K$ *and* $\bar{\mathbf{B}}_K$ *denote the rest-mass density, specific enthalpy, and magnetic field corresponding to* $\bar{\mathbf{U}}_K$*, respectively.*

For better legibility, the proof of Theorem 4.2 is presented in Appendix B.

4.3 The PCP limiting operator $\boldsymbol{\Pi}_h$

We now present the PCP limiting operator $\boldsymbol{\Pi}_h : \overline{\mathbb{G}}_h^k \longrightarrow \mathbb{G}_h^k$, which limits the numerical solutions from $\overline{\mathbb{G}}_h^k$ to $\mathbb{G}_h^k$ via a simple scaling PCP limiter [46, 48] as extension of the positivity-preserving limiter [54]. For any $\mathbf{U}_h \in \overline{\mathbb{G}}_h^k$, we construct the limited solution $\boldsymbol{\Pi}_h\mathbf{U}_h =: \widetilde{\mathbf{U}}_h \in \mathbb{G}_h^k$ as follows.

Let $\mathbf{U}_h\big|_K =: \mathbf{U}_K(\boldsymbol{x})$. Note $\bar{\mathbf{U}}_K \in \mathcal{G} = \mathcal{G}_1,\ \forall K \in \mathcal{T}_h$. To avoid the effect of the rounding error, a sufficiently small positive number ϵ is introduced such that $\bar{\mathbf{U}}_K \in \mathcal{G}_\epsilon$ for all $K \in \mathcal{T}_h$, where $\mathcal{G}_\epsilon = \big\{\mathbf{U} = (D, \mathbf{m}, \mathbf{B}, E)^\top :\ D \geq \epsilon,\ q(\mathbf{U}) \geq \epsilon,\ \Psi_\epsilon(\mathbf{U}) \geq 0\big\}$ is a convex set [46], with $\Psi_\epsilon(\mathbf{U}) := \Psi(\mathbf{U}_\epsilon)$ and $\mathbf{U}_\epsilon := \big(D, \mathbf{m}, \mathbf{B}, E - \epsilon\big)^\top$.

For each K, to construct $\widetilde{\mathbf{U}}_K(\boldsymbol{x}) := \widetilde{\mathbf{U}}_h\big|_K$, we proceed as follows [46]. First, we define

$$\widehat{\mathbf{U}}_K(\boldsymbol{x}) := \big(\widehat{D}_K(\boldsymbol{x}), \mathbf{m}_K(\boldsymbol{x}), \mathbf{B}_K(\boldsymbol{x}), E_K(\boldsymbol{x})\big)^\top$$

with $\widehat{D}_K(\boldsymbol{x}) = \theta_1\big(D_K(\boldsymbol{x}) - \bar{D}_K\big) + \bar{D}_K$, and $\theta_1 = \min\big\{1, (\bar{D}_K - \epsilon)/\big(\bar{D}_K - \min\limits_{\boldsymbol{x}\in\mathbb{S}_K} D_K(\boldsymbol{x})\big)\big\}$. Then, we define

$$\check{\mathbf{U}}_K(\boldsymbol{x}) := \big(\theta_2(\widehat{D}_K(\boldsymbol{x}) - \bar{D}_K) + \bar{D}_K,\ \theta_2\big(\mathbf{m}_K(\boldsymbol{x}) - \bar{\mathbf{m}}_K\big) + \bar{\mathbf{m}}_K,\ \mathbf{B}_K(\boldsymbol{x}),\ \theta_2\big(E_K(\boldsymbol{x}) - \bar{E}_K\big) + \bar{E}_K\big)^\top$$

with $\theta_2 = \min\big\{1, \big(q(\bar{\mathbf{U}}_K) - \epsilon\big)/\big(q(\bar{\mathbf{U}}_K) - \min\limits_{\boldsymbol{x}\in\mathbb{S}_K} q(\check{\mathbf{U}}_K(\boldsymbol{x}))\big)\big\}$. Finally, we define

$$\widetilde{\mathbf{U}}_K(\boldsymbol{x}) = \theta_3\big(\check{\mathbf{U}}_K(\boldsymbol{x}) - \bar{\mathbf{U}}_K\big) + \bar{\mathbf{U}}_K, \tag{54}$$

where $\theta_3 = \min\limits_{\boldsymbol{x}\in\mathbb{S}_K} \tilde{\theta}(\boldsymbol{x})$. Here $\tilde{\theta}(\boldsymbol{x}) = 1$ if $\Psi_\epsilon(\check{\mathbf{U}}_K(\boldsymbol{x})) \geq 0$; otherwise $\tilde{\theta}(\boldsymbol{x}) \in [0, 1)$ solves $\Psi_\epsilon\big((1-\tilde{\theta})\bar{\mathbf{U}}_K + \tilde{\theta}\check{\mathbf{U}}_K(\boldsymbol{x})\big) = 0$, which has a unique solution for the unknown $\tilde{\theta} \in [0, 1)$.

Lemma 4.2. *For any $\mathbf{U}_h \in \overline{\mathbb{G}}_h^k$, one has $\boldsymbol{\Pi}_h\mathbf{U}_h = \widetilde{\mathbf{U}}_h \in \mathbb{G}_h^k$.*

Proof. The above procedure indicates that, for $\forall K \in \mathcal{T}_h$, the limited solution defined by (54) satisfies $\widetilde{\mathbf{U}}_K(\boldsymbol{x}) \in \mathcal{G}_\epsilon \subset \mathcal{G}_1 = \mathcal{G},\ \forall \boldsymbol{x} \in \mathbb{S}_K$, and $\frac{1}{|K|}\int_K \widetilde{\mathbf{U}}_K d\boldsymbol{x} = \bar{\mathbf{U}}_K$. Besides, the limited magnetic field $\widetilde{\mathbf{B}}_K(\boldsymbol{x})$ keeps locally divergence-free within K. ■

Remark 4.3. *Notice that the PCP limiter is valid only when the numerical solutions are preserved in $\overline{\mathbb{G}}_h^k$. This requirement is guaranteed by the weak positivity property of our DG methods proven in Theorem 4.1, which does not hold for the standard DG methods for the conservative RMHD system (1) as shown in [46, 48] due to the effect of nonzero divergence error. The PCP limiting operator $\boldsymbol{\Pi}_h$ keeps both the conservativeness (32) and the high-order accuracy as shown in [53, 54, 52].*

4.4 The PCP property of fully discrete schemes

The PCP property of our fully discrete Runge-Kutta DG schemes (33) is proven in the following theorems.

Theorem 4.3. *Assume that* $\mathbf{U}_h^{(0)} = \mathbf{U}_h^n \in \mathbb{G}_h^k$, *then the solutions* $\mathbf{U}_h^{(i)}$ *at the* i*th Runge-Kutta stage,* $1 \le i \le N_r$, *computed by the proposed DG schemes* (33), *belong to* $\mathbb{G}_h^k$, *under the CFL condition*

$$\Delta t_n < \min_{i,\ell} \frac{\varpi_{\mathscr{E}}^{(q)} |K|}{\beta_{i\ell}\omega_q \left(a + \sigma_{K,\mathscr{E},q}(\mathbf{U}_h^{(i)})\right) |\mathscr{E}|}, \quad 1 \le q \le Q, \forall \mathscr{E} \in \partial K, \forall K \in \mathcal{T}_h. \tag{55}$$

Proof. We prove it by the second principle of mathematical induction for i. The hypothesis implies $\mathbf{U}_h^{(i)} \in \mathbb{G}_h^k$ for $i = 0$. Assume that $\mathbf{U}_h^{(\ell)} \in \mathbb{G}_h^k$, $1 \le \ell \le i-1$. Thanks to the weak PCP property (31) in Theorem 4.1, we have $\mathbf{U}_h^{(\ell)} + \beta_{i\ell}\Delta t_n \mathbf{L}_h(\mathbf{U}_h^{(\ell)}) \in \overline{\mathbb{G}}_h^k$, $1 \le \ell \le i-1$ under the CFL condition (55). The convexity of $\overline{\mathbb{G}}_h^k$ in Lemma 4.1 implies $\sum_{\ell=0}^{i-1} \left[\alpha_{i\ell}\big(\mathbf{U}_h^{(\ell)} + \beta_{i\ell}\Delta t_n \mathbf{L}_h(\mathbf{U}_h^{(\ell)})\big)\right] \in \overline{\mathbb{G}}_h^k$. Since the operator $\mathbf{\Pi}_h$ maps the numerical solutions from $\overline{\mathbb{G}}_h^k$ to $\mathbb{G}_h^k$, we obtain $\mathbf{U}_h^{(i)} \in \mathbb{G}_h^k$ by (33). Using the principle of induction, we have $\mathbf{U}_h^{(i)} \in \mathbb{G}_h^k$ for all $i \in \{0, 1, \ldots, N_r\}$. ■

Theorem 4.4. *Under the CFL condition* (55), *the proposed fully discrete Runge-Kutta DG schemes* (33) *always preserves* $\mathbf{U}_h^n \in \mathbb{G}_h^k$ *for all* $n \in \mathbb{N}$.

Proof. Since $\mathbf{P}_w(\mathbf{U}(\boldsymbol{x}, 0)) \in \overline{\mathbb{G}}_h^k$ as indicated by Lemma 4.1, we known $\mathbf{U}_h^0 \in \mathbb{G}_h^k$. With the help of Theorem 4.3, we obtain the conclusion by induction for n. ■

4.5 Illustration of some details on Cartesian meshes

Assume that the mesh consists of rectangular cells $\{[x_{i-1/2}, x_{i+1/2}] \times [y_{\ell-1/2}, y_{\ell+1/2}]\}$, and define $\Delta x_i = x_{i+1/2} - x_{i-1/2}$ and $\Delta y_\ell = y_{\ell+1/2} - y_{\ell-1/2}$ as the spatial step-sizes. Let $\mathbb{S}_i^x = \{x_i^{(q)}\}_{q=1}^Q$ and $\mathbb{S}_\ell^y = \{y_\ell^{(q)}\}_{q=1}^Q$ be the set of Gauss quadrature nodes in $[x_{i-1/2}, x_{i+1/2}]$ and $[y_{\ell-1/2}, y_{\ell+1/2}]$ respectively. For a rectangular cell $K = [x_{i-1/2}, x_{i+1/2}] \times [y_{\ell-1/2}, y_{\ell+1/2}]$, the point set $\breve{\mathbb{S}}_K$ involved in (41) is $\mathbb{S}_i^x \otimes \mathbb{S}_\ell^y$, and the set $\widehat{\mathbb{S}}_K$ is given by (cf. [53])

$$\widehat{\mathbb{S}}_K = \big(\widehat{\mathbb{S}}_i^x \otimes \mathbb{S}_\ell^y\big) \cup \big(\mathbb{S}_i^x \otimes \widehat{\mathbb{S}}_\ell^y\big), \tag{56}$$

where $\widehat{\mathbb{S}}_i^x = \{\widehat{x}_i^{(\mu)}\}_{\mu=1}^{\mathtt{L}}$ and $\widehat{\mathbb{S}}_\ell^y = \{\widehat{y}_\ell^{(\mu)}\}_{\mu=1}^{\mathtt{L}}$ denote the $\mathtt{L}$-point ($\mathtt{L} \ge \frac{k+3}{2}$) Gauss–Lobatto quadrature nodes in the intervals $[x_{i-1/2}, x_{i+1/2}]$ and $[y_{\ell-1/2}, y_{\ell+1/2}]$ respectively. With $\widehat{\mathbb{S}}_K$ in (56), a special quadrature [53] satisfying (40) can be constructed:

$$\begin{aligned}
\frac{1}{|K|}\int_K u(\boldsymbol{x})\mathrm{d}\boldsymbol{x} = &\sum_{q=1}^{Q} \frac{\Delta x_i \widehat{\omega}_1 \omega_q}{\Delta x_i + \Delta y_\ell}\left(u\big(x_i^{(q)}, y_{\ell-\frac{1}{2}}\big) + u\big(x_i^{(q)}, y_{\ell+\frac{1}{2}}\big)\right) \\
&+ \sum_{q=1}^{Q} \frac{\Delta y_\ell \widehat{\omega}_1 \omega_q}{\Delta x_i + \Delta y_\ell}\left(u\big(x_{i-\frac{1}{2}}, y_\ell^{(q)}\big) + u\big(x_{i+\frac{1}{2}}, y_\ell^{(q)}\big)\right) \\
&+ \sum_{\mu=2}^{\mathtt{L}-1}\sum_{q=1}^{Q} \frac{\Delta x_i \widehat{\omega}_\mu \omega_q}{\Delta x_i + \Delta y_\ell} u\big(x_i^{(q)}, \widehat{y}_\ell^{(\mu)}\big) \\
&+ \sum_{\mu=2}^{\mathtt{L}-1}\sum_{q=1}^{Q} \frac{\Delta y_\ell \widehat{\omega}_\mu \omega_q}{\Delta x_i + \Delta y_\ell} u\big(\widehat{x}_i^{(\mu)}, y_\ell^{(q)}\big), \qquad \forall u \in \mathbb{P}^k(K),
\end{aligned} \tag{57}$$

where $\{\widehat{w}_\mu\}_{\mu=1}^{\mathtt{L}}$ denote the quadrature weights of the $\mathtt{L}$-point Gauss–Lobatto quadrature rule. If we label the top, left, bottom and right edges of K as $\mathscr{E}_1$, $\mathscr{E}_2$, $\mathscr{E}_3$ and $\mathscr{E}_4$, respectively, then (57) implies $\varpi_{\mathscr{E}_j}^{(q)} = \frac{\Delta x_i \widehat{\omega}_1 \omega_q}{\Delta x_i + \Delta y_\ell}$, $j = 1, 3$; $\varpi_{\mathscr{E}_j}^{(q)} = \frac{\Delta y_\ell \widehat{\omega}_1 \omega_q}{\Delta x_i + \Delta y_\ell}$, $j = 2, 4$. According to Theorem 4.3, we rewrite the CFL condition (55) for the proposed PCPDG schemes on Cartesian meshes as

$$\Delta t_n \left(\frac{1}{\Delta x_i} + \frac{1}{\Delta y_\ell} \right) < \min_{m,s,q} \frac{\widehat{\omega}_1}{\beta_{ms} \big(a + \sigma_{K,\mathscr{E}_j,q}(\mathbf{U}_h^{(m)}) \big)}, \quad \forall K \in \mathcal{T}_h,\ 1 \le j \le 4, \tag{58}$$

where $\widehat{\omega}_1 = \frac{1}{\mathtt{L}(\mathtt{L}-1)}$. Since $\sigma_{K,\mathscr{E}_j,q}(\mathbf{U}_h^{(m)})$ depends on the numerical solutions at intermediate Runge-Kutta stages, it can be difficult to rigorously enforce the condition (58). However, note that $\sigma_{K,\mathscr{E}_j,q}(\mathbf{U}_h^{(m)})$ is proportional to the jump of the normal component of the magnetic field on the edge $\mathscr{E}_j$. Since the jump is zero for the exact solution, $\sigma_{K,\mathscr{E}_j,q}$ is small and at the level of truncation error in smooth region; while, for problems involving shocks or contact discontinuities, some numerical evidence in Sections 5.2–5.4 indicates that $\sigma_{K,\mathscr{E}_j,q}$ is small compared to a. Therefore, the theoretical CFL condition (58) is acceptable. In practical computations, evaluating $\sigma_{K,\mathscr{E}_j,q}$ is computationally expensive and unnecessary; we suggest

$$\Delta t_n = \frac{C_{\mathrm{cfl}}}{a \max_{m,s} \beta_{ms}} \left(\frac{1}{\Delta x_i} + \frac{1}{\Delta y_\ell} \right)^{-1}$$

with the CFL number C_{cfl} (slightly) smaller than $\widehat{\omega}_1$, which works robustly in our numerical tests. For the third-order SSP Runge-Kutta method (34), $\max_{m,s} \beta_{ms} = 1$.

Remark 4.4. *Notice that the equations (39) can also be derived from a semi-discrete finite volume method for the system (10), if the approximate solution function $\mathbf{U}_h(\boldsymbol{x})$, or its values at the quadrature points, are reconstructed from the cell averages $\{\bar{\mathbf{U}}_K\}$ using some high-order reconstruction techniques such as the ENO (essentially non-oscillatory) and the WENO (weighted ENO) approaches with the locally divergence-free property being taken into account. Therefore, our numerical PCP framework and analyses can be directly used to design PCP high-order finite volume methods for (10).*

5 Numerical tests

In this section, we present the numerical tests on 2D uniform Cartesian meshes for several demanding RMHD problems, which involve either small plasma-beta $\beta := p/p_m$, strong discontinuities, or low p or ρ, to validate the theoretical PCP property and the effectiveness of our PCP methods. We only show the numerical results of the PCP third-order accurate ($k = 2$) DG scheme, which is representative and without loss of generality, with the third-order SSP Runge-Kutta method (33)–(34) for time discretization. We set the CFL number as 0.15, and unless otherwise stated, the ideal EOS (3) with $\Gamma = 5/3$ will be used.

5.1 Smooth problems

To verify the accuracy of our method we test two smooth problems. The first is analogous to those tested in [45, 30], and it involves very low density and low pressure; the exact solution is

$$(\rho, \mathbf{v}, \mathbf{B}, p)(x, y, t) = (1 + 0.9999999 \sin\big(2\pi(x + y - 1.1t)\big), 0.9, 0.2, 0, 1, 1, 1, 10^{-2}),$$

describing the propagation of a RMHD sine wave in the computational domain $\Omega = [0, 1]^2$ with a large velocity $|\mathbf{v}| \approx 0.922c$. The second problem describes Alfvén waves propagating periodically in $\Omega = [0, \sqrt{2}]^2$ with a speed of $0.9c$ much higher than that in [57], and the exact solution is

$$\begin{aligned}
&\rho(x, y, t) = 1, \quad p(x, y, t) = 0.1, \quad v_1(x, y, t) = -0.9 \sin(2\pi(\varsigma + t/\kappa)) \sin\alpha, \\
&v_2(x, y, t) = 0.9 \sin(2\pi(\varsigma + t/\kappa)) \cos\alpha, \quad v_3(x, y, t) = 0.9 \cos(2\pi(\varsigma + t/\kappa)), \\
&B_1(x, y, t) = \cos\alpha + \kappa v_1(x, y, t), \quad B_2(x, y, t) = \sin\alpha + \kappa v_2(x, y, t), \quad B_3(x, y, t) = \kappa v_3(x, y, t),
\end{aligned}$$

where $\kappa = \sqrt{1 + \rho HW^2}$ and $\varsigma = x \cos\alpha + y \sin\alpha$ with $\alpha = \pi/4$.

In the computations, the domain Ω is partitioned into $N \times N$ uniform rectangular cells with $N \in \{10, 20, 40, 80, 160, 320, 640\}$, and periodic boundary conditions are used. Fig. 1 shows the errors at $t = 1$ in the numerical solutions computed by the PCP third-order DG method on meshes with several different N. It is seen that the magnitudes of the errors are reduced as we refine the mesh. Moreover, the expected third-order convergence rate is observed, indicating that our discretization of the added source term in the symmetrizable RMHD system (10) and the PCP limiting procedure both maintain the desired accuracy, as expected.

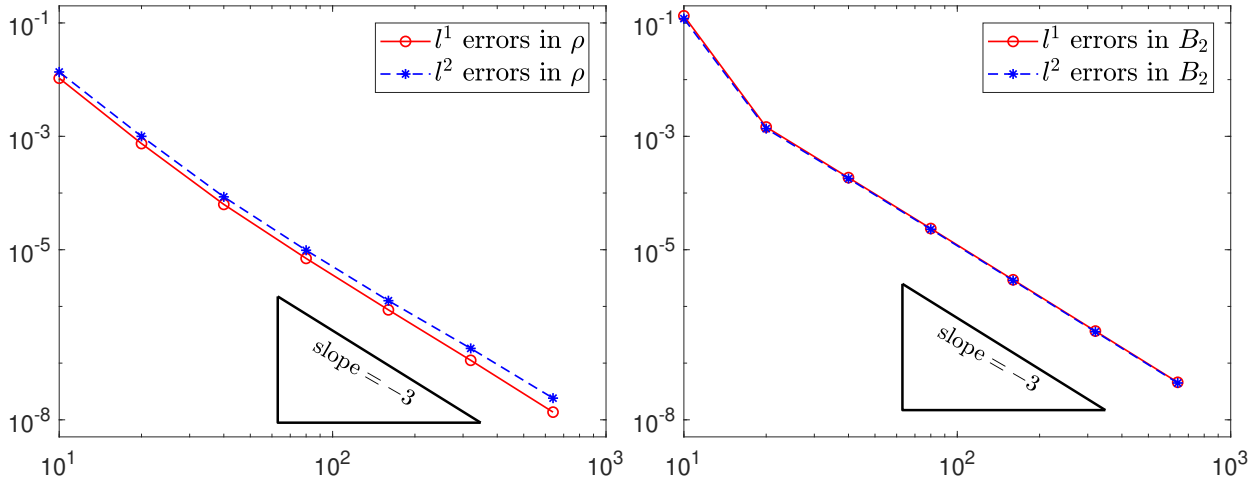

Figure 1: Numerical errors in l^1 and l^2 norms at $t = 1$ for the first smooth problem (left) and the second smooth problem (right). The horizontal axis corresponds the value of N.

In what follows, we will verify the capability of our PCP methods in resolving complicated flow structures, by simulating an Orszag-Tang problem, three blast problems and two astrophysical jets. Because these problems involve (strong) discontinuities, we need to apply some nonlinear limiters to suppress the undesirable oscillations in the high-order DG solutions and

enhance the numerical stability. To this end, we use a locally divergence-free WENO limiter [31, 57] right before the PCP limiting procedure. The WENO limiter is applied only within some "trouble" cells that are identified adaptively by the KXRCF shock detector [21].

5.2 Orszag-Tang problem

This test simulates an Orszag-Tang problem for the RMHD. We use a setup same as in [38]. The computational domain is $\Omega = [0, 2\pi]^2$ with periodic boundary conditions. It is initially filled with hot gas with $\rho = 1$ and $p = 10$. The initial velocity field is $\mathbf{v}(x, y, 0) = (-A\sin(y), A\sin(x), 0)$, where we set $A = 0.99/\sqrt{2}$ such that the maximum velocity is $0.99c$ (corresponding to the Lorentz factor ≈ 7.09). The adiabatic index is set as $\Gamma = 4/3$ in this example. The initial magnetic field is $\mathbf{B}(x, y, 0) = (-\sin y, \sin(2x), 0)$. Although the initial solution is very smooth, complex wave structures will develop as time increases, eventually producing turbulence behavior. The numerical results computed by our PCP method on 600×600 uniform grids are presented Fig. 2. One can observe that the complicated flow structures are correctly captured and agree with those presented in [38, 44]. In this test, we observe that it is necessary to enforce the DG solution in $\mathbb{G}_n^k$ by the PCP limiting procedure, otherwise the code would break down at time $t \approx 1.98$.

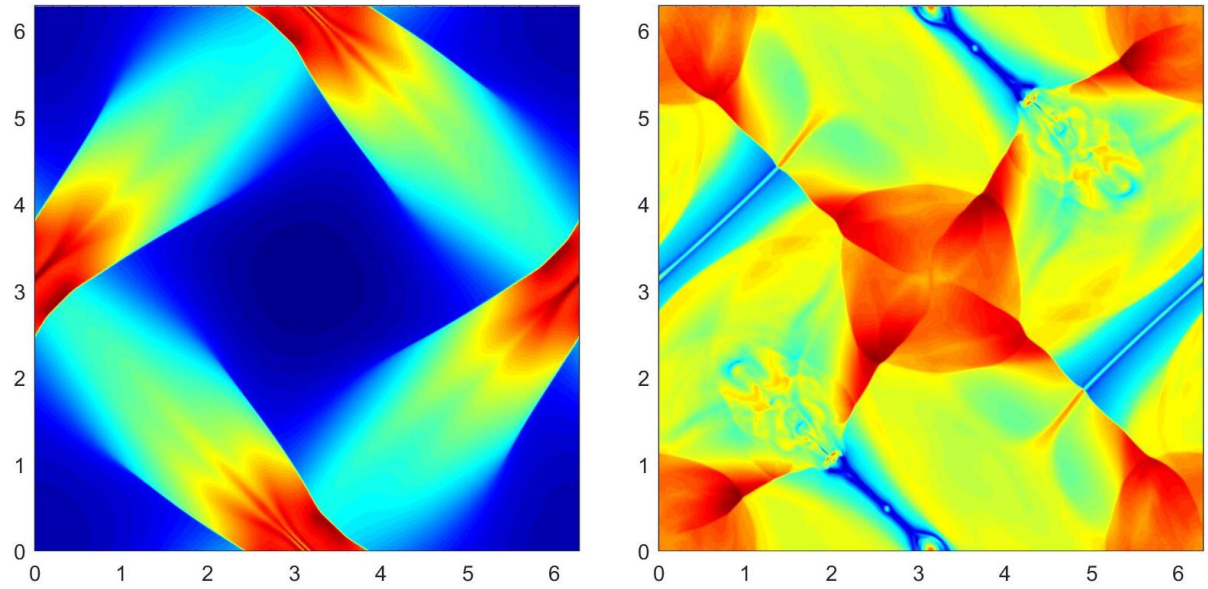

Figure 2: Schlieren images of $\log(\rho)$ at $t = 2.818127$ (left) and $t = 6.8558$ (right) for the Orszag-Tang problem.

We follow [7, 38] and quantitatively study the divergence error in the numerical magnetic field $\mathbf{B}_h$. For the DG finite element methods, a standard way to measure the global divergence error was proposed in [7], as defined by

$$\|\nabla \cdot \mathbf{B}_h\|_{\star,h} := \sum_{\mathscr{E} \in \mathcal{T}_h} \int_{\mathscr{E}} |[\![\langle \mathbf{n}_{\mathscr{E}}, \mathbf{B}_h \rangle]\!]| \, \mathrm{d}s + \sum_{K \in \mathcal{T}_h} \int_K |\nabla \cdot \mathbf{B}_h| \, \mathrm{d}\boldsymbol{x},$$

where $[\![\langle \mathbf{n}_{\mathscr{E}}, \mathbf{B}_h \rangle]\!]$ denotes the jump of the normal component of $\mathbf{B}_h$ on the edge $\mathscr{E}$. We then define the global relative divergence error as

$$\varepsilon_{\text{div}} := \frac{\|\nabla \cdot \mathbf{B}_h\|_{\star,h}}{\|\mathbf{B}_h\|_{\star,h}} \tag{59}$$

with

$$\|\mathbf{B}_h\|_{\star,h} := \sum_{\mathscr{E} \in \mathcal{T}_h} \int_{\mathscr{E}} |\mathbf{B}_h| \, \mathrm{d}s + \sum_{K \in \mathcal{T}_h} \int_K |\mathbf{B}_h| \, \mathrm{d}\boldsymbol{x}.$$

In Fig. 3(a), we plot ε_{div} against time t. It is observed that, at the initial stage ($t < 1.5$) ε_{div} is very small as the solution is initially smooth, and, during the entire simulation, the magnitude of ε_{div} is kept at order $\mathcal{O}(10^{-3})$.

To justify that the theoretically estimated CFL condition (58) is acceptable, we compute the maximum value of $\sigma_{K,\mathscr{E},q}$ on the entire mesh and plot its temporal evolution in Fig. 3(b). It indicates that, during the simulation, $\sigma_{K,\mathscr{E},q}$ is relatively small compared to $a = c = 1$, so that its effect in (58) is small and does not lead to strict restriction on the time step-sizes.

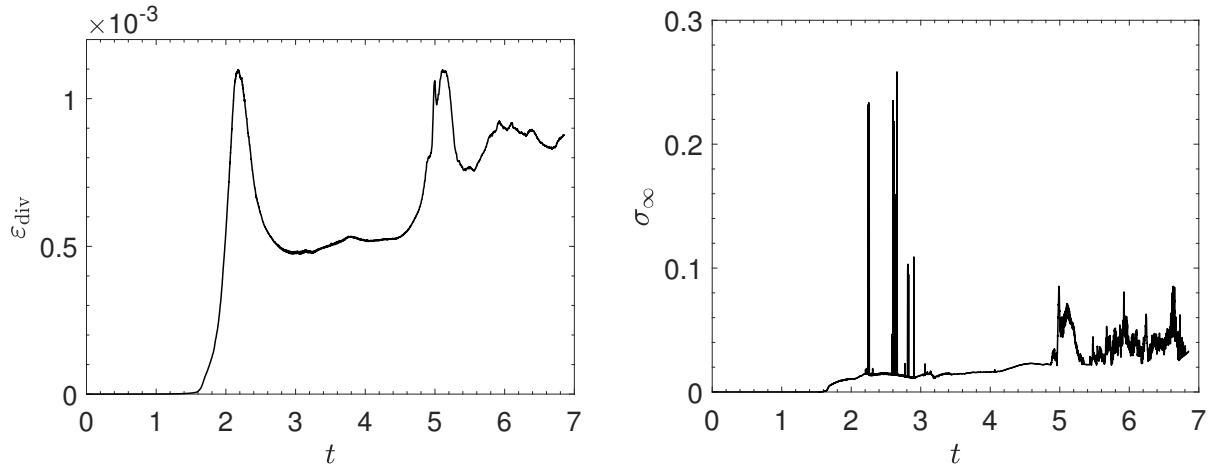

(a) global (relative) divergence error ε_{div} (b) $\sigma_\infty := \max_{K,\mathscr{E},q} \sigma_{K,\mathscr{E},q}$

Figure 3: Time evolution of the (relative) divergence error ε_{div} and the maximum value of $\sigma_{K,\mathscr{E},q}$ in the CFL condition (58) for the Orszag-Tang problem.

5.3 Blast problems

This is a benchmark test for RMHD codes. Simulating a RMHD blast problem with strong magnetic field is known to be difficult, because nonphysical quantities, e.g., negative thermal pressure, can be produced easily in the numerical simulation. Our setup is similar to those in [26, 10, 2, 51]. Initially, the fluid in the computational domain $\Omega = [-6, 6]^2$ is at rest. Let $r := \sqrt{x^2 + y^2}$. The domain Ω contains an internal cylindrical region ($r < 0.8$) centered at the origin with $\rho_i = 10^{-2}$ and $p_i = 1$, and the ambient medium region ($r > 1$) with low density ($\rho_a = 10^{-4}$) and low pressure ($p_a = 5 \times 10^{-4}$). Between the two regions, the values of the density

and pressure are reached by linear interpolation for $r \in [0.8, 1]$ as in [26, 10, 2, 51]. We take the adiabatic index as $\Gamma = 4/3$ in this test. The initial magnetic field is a uniform constant vector $(B_a, 0, 0)$. As B_a is set larger, the plasma beta $\beta_a := p_a/p_m$ becomes lower, and the simulation of this test is more challenging. In the literature [26, 10, 2], a moderately magnetized case with $B_a = 1$ (corresponding $\beta_a = 0.1$) is widely simulated. Zanotti et al. tested a more strongly magnetized case with $B_a = 0.5$ (a lower plasma-beta $\beta_a = 4 \times 10^{-3}$) in [51]. Many existing methods in the literature require some artificial treatments for the strongly magnetized cases; see e.g., [20, 26, 10]. It was reported in [10] that, if no ad hoc numerical strategy was employed, the RMHD code, `ECHO`, could not run this test with $B_a > 0.1$.

In order to examine the robustness and the PCP property of the proposed method, we perform this test with different $B_a \in \{0.1, 0.5, 20, 100, 2000\}$. These five configurations include the two cases in the literature [26, 10, 2, 51] and three much more challenging cases. Our computations are performed on the mesh of 400×400 uniform cells. It is observed that our PCP methods are able to successfully simulate all these test cases without using any artificial treatments. Fig. 4 shows our numerical results at $t = 4$, for three different magnetizations, corresponding to a moderate magnetic field $B_a = 0.1$, a relatively strong magnetic field $B_a = 0.5$, and a extremely strong magnetic field $B_a = 2000$, respectively. Our numerical results for the first two cases are in good agreement with those reported in [51, 2, 46]. The wave patterns for $B_a = 20$ and $B_a = 100$ are similar to that for $B_a = 2000$ and thus omitted here.

As far as we know, successful simulations of such an extreme RMHD blast test with $B_a = 2000$ and so low plasma-beta ($\beta_a = 2.5 \times 10^{-10}$) have not been reported in the literature. We also observe that, if we turn off the PCP limiter in the strongly magnetized tests ($B_a \geq 0.5$), nonphysical numerical solutions exceeding the set $\mathbb{G}_n^k$ will appear in the simulations, and the DG code will break down. We have also tried to perform the above simulations by dropping the discrete symmetrization source term $\mathcal{J}_K^{(2)}(\mathbf{U}_h, \mathbf{u})$ in our scheme (37) while keeping the WENO and PCP limiters employed. This actually corresponds to using the locally divergence-free DG scheme [22, 57] with the WENO and PCP limiters for the conservative RMHD system (1). It is noticed that this scheme, in theory, is not PCP [46], and, as expected, is not able to run the tests with $B_a \in \{100, 2000\}$. This demonstrates the importance and necessity of including the suitably discretized symmetrization source term for achieving the desired PCP property of the DG schemes.

Fig. 5 shows the temporal evolution of the global relative divergence error ε_{div} defined in (59). It is seen, for such strong blast problems with shocks, that the relative divergence errors remain at relatively small levels during the whole simulations, as desired. The temporal evolution of the maximum value of $\sigma_{K,\mathscr{E},q}$ is displayed in Fig. 6 for the three blast problems. It indicates that $\sigma_{K,\mathscr{E},q} \ll a = 1$. This, again, demonstrates that $\sigma_{K,\mathscr{E},q}$ has a little effect in the theoretical CFL condition (58) and thus does not cause strict restriction on the time step-sizes.

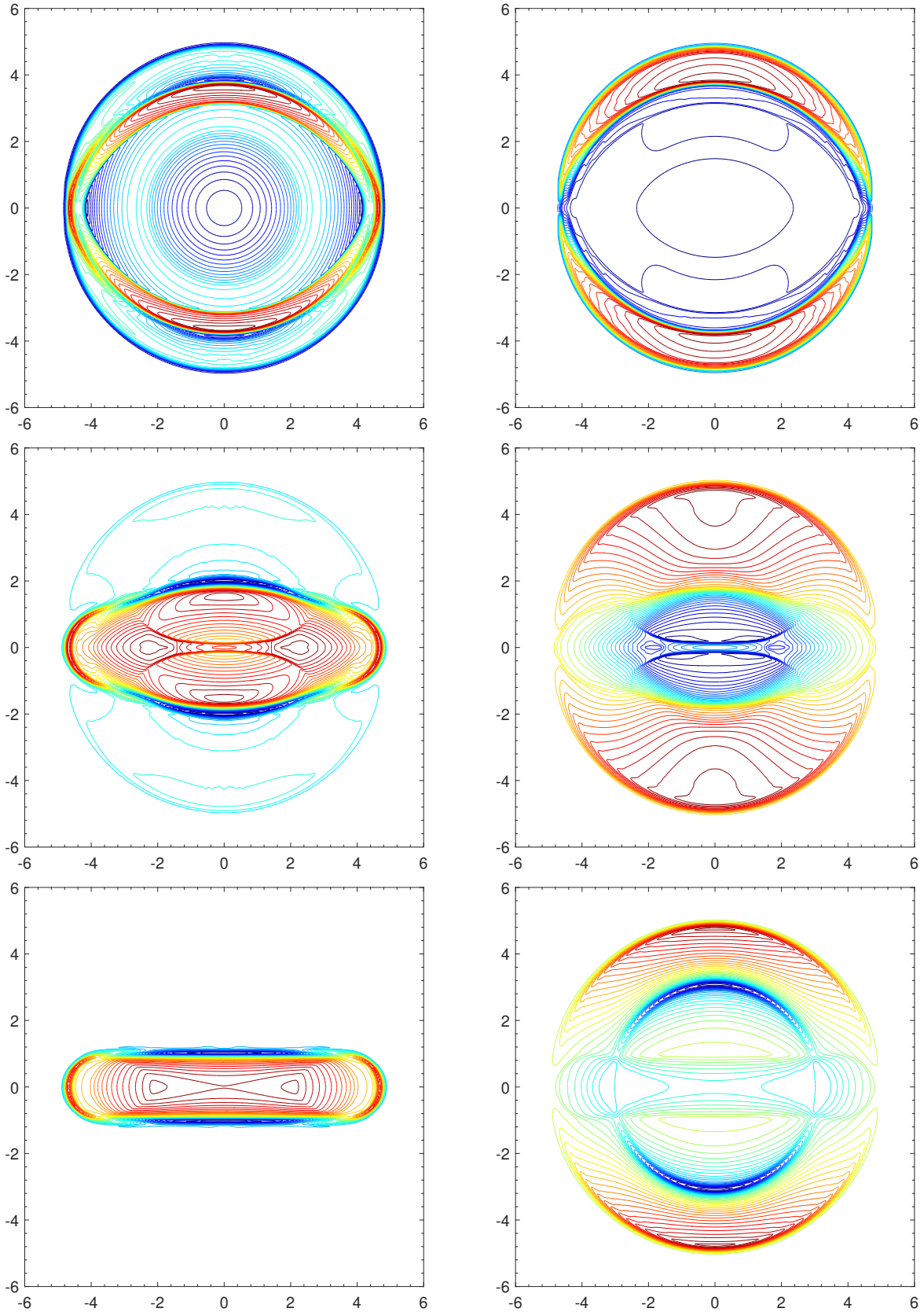

Figure 4: Contour plots of $\log(\rho)$ (left) and $|\mathbf{B}|$ (right) for the blast problems at $t = 4$. Forty equally spaced contour lines are displayed. Top: the moderately magnetized case ($B_a = 0.1$, $\beta_a = 0.1$); middle: the relatively strongly magnetized case ($B_a = 0.5$, $\beta_a = 4 \times 10^{-3}$); bottom: the extremely strongly magnetized case ($B_a = 2000$, $\beta_a = 2.5 \times 10^{-10}$).

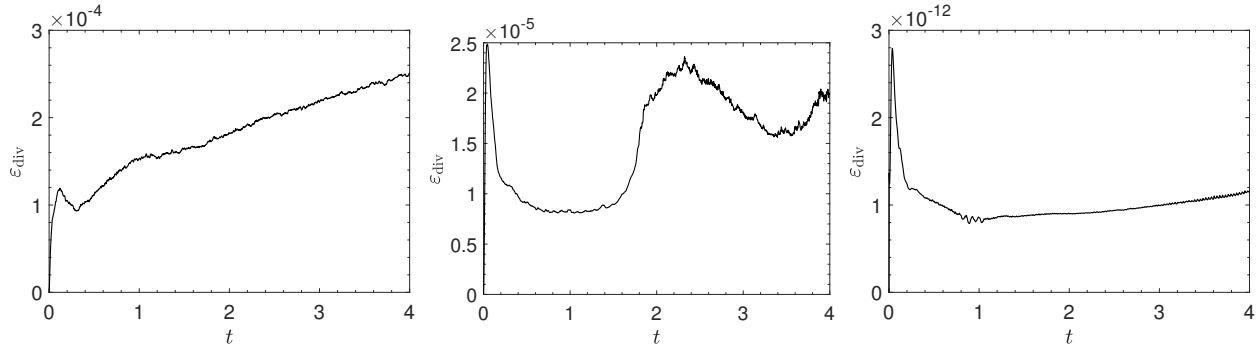

Figure 5: Time evolution of the global (relative) divergence error ε_{div} for the three blast problems. Left: the moderately magnetized case ($B_a = 0.1$); middle: the relatively strongly magnetized case ($B_a = 0.5$); right: the extremely strongly magnetized case ($B_a = 2000$).

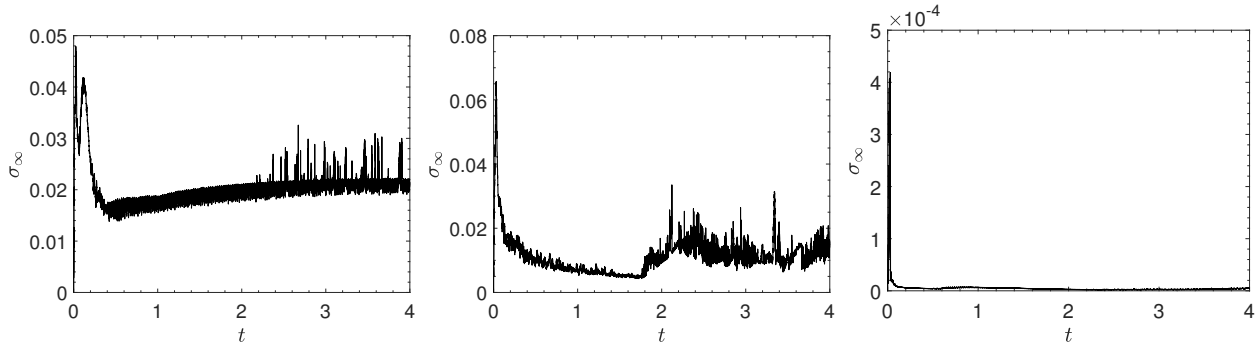

Figure 6: Time evolution of $\sigma_\infty := \max_{K,\mathscr{E},q} \sigma_{K,\mathscr{E},q}$ for the three blast problems. Left: the moderately magnetized case ($B_a = 0.1$); middle: the relatively strongly magnetized case ($B_a = 0.5$); right: the extremely strongly magnetized case ($B_a = 2000$).

5.4 Astrophysical jets

In this test, we perform simulations of two relativistic jets, where the internal energy is exceedingly small compared to the kinetic energy so that negative thermal pressure can be easily generated in numerical computations. Moreover, the high-speed jet flows may involve strong shock wave, interface instability, and shear flow, leading to their successful simulation difficult; see, e.g., [54, 45, 30, 47, 42].

We simulate the RMHD jet flows by adding a magnetic field to a pressure-matched highly supersonic RHD jet model from [47]. The domain $[-12, 12] \times [0, 25]$ is initially filled with a uniform medium with $\mathbf{v} = \mathbf{0}$ and $\rho = 1$. In the y-direction, a RMHD jet of Mach number $M_b = 50$ is injected into the domain with a density of $\rho_b = 0.1$, a speed of $v_b = 0.99c$, and a pressure equaling the ambient pressure. This inflow condition is enforced at the jet nozzle $\{(x, y) : |x| \leq 0.5, y = 0\}$ on the bottom boundary, while the other boundary conditions are outflow. For this problem, the corresponding initial Lorentz factor $W \approx 7.09$, and one can compute the relativistic Mach number as $M_r := M_b W / W_s \approx 354.37$, where W_s stands for the Lorentz factor of the local sound speed. The exceedingly high Mach number and large Lorentz factor cause the simulation of this problem very challenging. Along the y-direction, a magnetic field $(0, B_a, 0)$ is initialized. The presence of the magnetic field renders the simulation of this test case more difficult. For comparison, we simulate a non-magnetized case with $B_a = 0$ and a strongly magnetized case with $B_a = \sqrt{2000p}$ (the corresponding plasma-beta $\beta_a = 10^{-3}$). We set the computational domain as $[0, 12] \times [0, 25]$ and divide it into 240×500 uniform cells with the reflecting boundary condition on $\{x = 0, 0 \leq y \leq 25\}$.

Fig. 7 shows the numerical $\log(\rho)$ within the domain $[-12, 12] \times [0, 25]$ at three different time instances for the non-magnetized case and the strongly magnetized case, respectively. The dynamics of the relativistic jets are clearly shown in those images. We see that, during the simulations, the Mach shock wave and the interfaces are well captured. The wave patterns for the non-magnetized case agree with those computed in [47]. Due to the effect of the strong magnetic field, the flow structures of the strongly magnetized case are obviously different from those of the non-magnetized case. The good robustness of the proposed PCP method is exhibited in such extreme tests. It is observed that if we turn off the PCP limiter, the simulation code can only be run for a few time steps and then breaks down as nonphysical numerical solutions are produced. In addition, when dropping the discrete symmetrization source term $\mathcal{J}_K^{(2)}(\mathbf{U}_h, \mathbf{u})$ in our scheme (37), we find the cell averages of the DG solutions will exceed the admissible state set $\mathcal{G}$ and the scheme will fail in the strongly magnetized test. Again, this demonstrates the importance of including the suitably discretized symmetrization source term for achieving the PCP property.

We measure the global divergence error by (59) for the magnetized jet problem and plot the error evolution in Fig. 8(a). It is observed that the global divergence error grows linearly in time but remains below 10^{-3} during the simulation. To demonstrate the theoretical CFL condition (58) is acceptable, we measure the maximum value of $\sigma_{K,\mathscr{E},q}$ on the entire mesh and show its evolution in Fig. 8(b). One can see that $\sigma_{K,\mathscr{E},q}$ is small compared to $a = c = 1$,

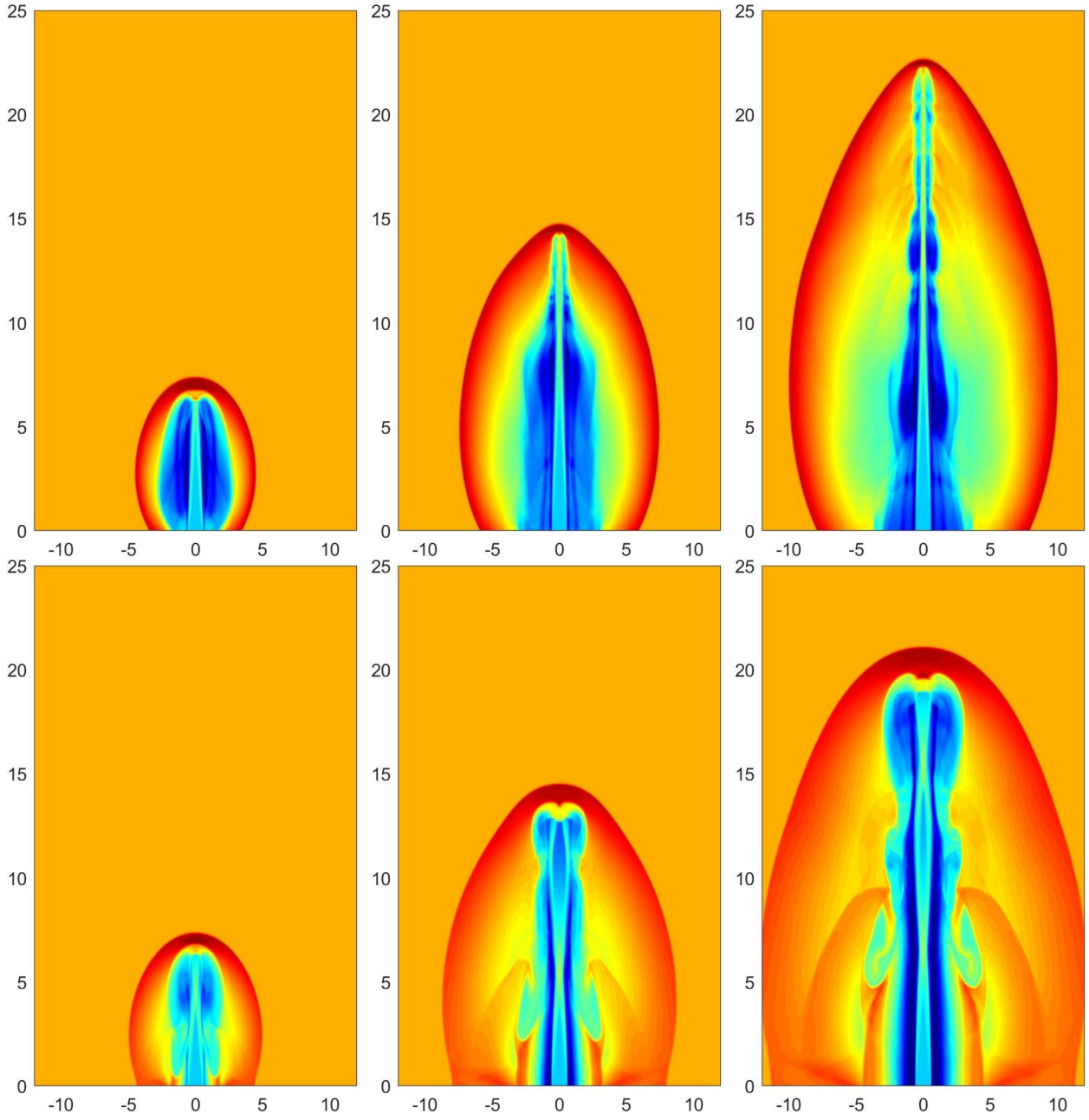

Figure 7: Schlieren images of $\log(\rho)$ for the relativistic jets at $t = 10$, 20, and 30 (from left to right). Top: the non-magnetized case; bottom: the strongly magnetized case.

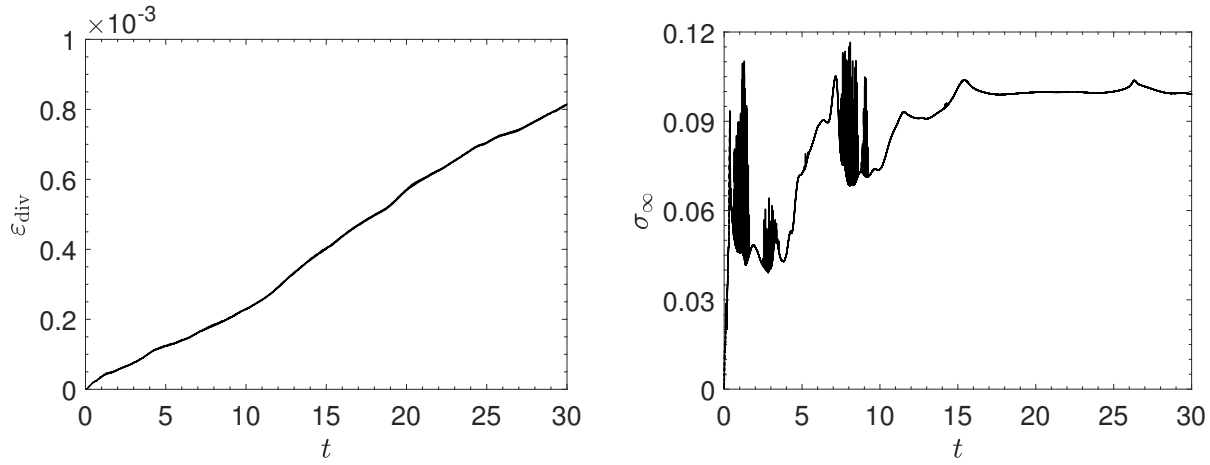

(a) global (relative) divergence error ε_{div} (b) $\sigma_\infty := \max_{K,\mathscr{E},q} \sigma_{K,\mathscr{E},q}$

Figure 8: Time evolution of the (relative) divergence error ε_{div} and the maximum value of $\sigma_{K,\mathscr{E},q}$ in the CFL condition (58) for the magnetized jet problem.

confirming that its effect in the CFL condition (58) does not lead to strict restriction on the time step-sizes.

6 Conclusions

We have proposed a framework of constructing provably PCP high-order accurate DG schemes for the multidimensional RMHD equations coupled with a general EOS on general meshes. The schemes are built on a suitable, locally divergence-free DG discretization of the recently proposed symmetrizable RMHD equations, which are discovered to accommodate the PCP property at the PDE level no matter the divergence-free condition is satisfied or not. The resulting DG schemes with SSP time discretizations are shown to satisfy a weak PCP property, which implies that a simple limiter can enforce the PCP property without losing conservation and high order accuracy. Most notably, we have rigorously proven the PCP property by using a novel "quasi-linearization" approach to handle the highly nonlinear physical constraints, technical splitting to offset the influence of divergence error, and sophisticated estimates to analyze the beneficial effect of the symmetrization source term. Several demanding numerical examples, including a strongly magnetized bast problem with extremely low plasma-beta (2.5×10^{-10}) and two highly supersonic RMHD jets, have been tested and demonstrated the robustness and effectiveness of the proposed PCP schemes. It is worth noting that our numerical PCP framework and analyses are also readily applicable for designing PCP high-order finite volume methods, as mentioned in Remark 4.4. In the context of RMHD, our results provide some new insights into eliminating the effect of nonzero divergence on the PCP property at both the PDE and numerical levels, showing the unity of continuous and discrete objects.

A Proof of Proposition 2.1

Due to the assumption that the exact smooth solution exists for $\boldsymbol{x} \in \mathbb{R}^d$ and $0 \le t \le T$, the Lorentz factor W does not blow up, and then $|\mathbf{v}(\boldsymbol{x},t)| < 1$ for $\forall \boldsymbol{x} \in \mathbb{R}^d$ and $0 \le t \le T$. For any $(\bar{\boldsymbol{x}},\bar{t}) \in \mathbb{R}^d \times \mathbb{R}^+$, we denote by $\boldsymbol{x} = \boldsymbol{x}(t;\bar{\boldsymbol{x}},\bar{t})$ the integral curve of $\frac{d\boldsymbol{x}}{dt} = \mathbf{v}(\boldsymbol{x},t)$ through the point $(\bar{\boldsymbol{x}},\bar{t})$. Define $\boldsymbol{x}_0(\bar{\boldsymbol{x}},\bar{t}) := \boldsymbol{x}(0;\bar{\boldsymbol{x}},\bar{t})$. It can be observed that the curve passes through the point $(\boldsymbol{x}_0(\bar{\boldsymbol{x}},\bar{t}),0)$ at the initial time $t = 0$. For strong solutions, we can reformulate the continuity equation of (10) for ρW as $\frac{\mathcal{D}(\rho W)}{\mathcal{D}t} = -\rho W \nabla \cdot \mathbf{v}$, where $\frac{\mathcal{D}}{\mathcal{D}t} := \frac{\partial}{\partial t} + \mathbf{v}(\boldsymbol{x},t)\nabla\cdot$ denotes the derivative along the integral curve. Integration of this reformulated continuity equation from $t = 0$ to $\bar{t}$ along the curve implies

$$\rho W(\bar{\boldsymbol{x}},\bar{t}) = \rho_0 W_0(\boldsymbol{x}_0(\bar{\boldsymbol{x}},\bar{t})) \exp\left(-\int_0^{\bar{t}} \nabla \cdot \mathbf{v}(\boldsymbol{x}(t;\bar{\boldsymbol{x}},\bar{t}),t)dt\right) > 0,$$

which, along with $W(\bar{\boldsymbol{x}},\bar{t}) \ge 1$, imply $\rho(\bar{\boldsymbol{x}},\bar{t}) > 0$ for all $(\bar{\boldsymbol{x}},\bar{t}) \in \mathbb{R}^3 \times \mathbb{R}^+$. For smooth solutions of the modified RMHD system (10), one can derive that

$$\frac{\mathcal{D}\left(p\rho^{-\Gamma}\right)}{\mathcal{D}t} = \frac{\partial}{\partial t}\left(p\rho^{-\Gamma}\right) + \mathbf{v}\cdot\nabla\left(p\rho^{-\Gamma}\right) = 0, \tag{60}$$

which implies $p\rho^{-\Gamma}(\bar{\boldsymbol{x}},\bar{t}) = p_0\rho_0^{-\Gamma}(\boldsymbol{x}_0(\bar{\boldsymbol{x}},\bar{t})) > 0$. It follows that $p(\bar{\boldsymbol{x}},\bar{t}) > 0,\ \forall\,(\bar{\boldsymbol{x}},\bar{t}) \in \mathbb{R}^3 \times \mathbb{R}^+$. Using the ideal EOS (3) with $\Gamma \in (1,2]$ gives $e(\bar{\boldsymbol{x}},\bar{t}) = \frac{1}{\Gamma-1}p(\bar{\boldsymbol{x}},\bar{t})/\rho(\bar{\boldsymbol{x}},\bar{t}) > 0, \forall\,(\bar{\boldsymbol{x}},\bar{t}) \in \mathbb{R}^3\times\mathbb{R}^+$. It has been shown in [44] that, for smooth solutions of (10), the quantity $\frac{\nabla\cdot\mathbf{B}}{\rho W}$ satisfies

$$\frac{\partial}{\partial t}\left(\frac{\nabla\cdot\mathbf{B}}{\rho W}\right) + \mathbf{v}\cdot\nabla\left(\frac{\nabla\cdot\mathbf{B}}{\rho W}\right) = 0,$$

which implies that $\frac{\nabla\cdot\mathbf{B}}{\rho W}$ remains constant along the integral curve $\boldsymbol{x} = \boldsymbol{x}(t;\bar{\boldsymbol{x}},\bar{t})$, and further yields (13). The proof is complete.

B Proof of Theorem 4.2

For the first-order DG method ($k = 0$), $\mathbf{U}_h|_K(\boldsymbol{x}) \equiv \bar{\mathbf{U}}_K$, $\forall K \in \mathcal{T}_h$, and

$$\begin{aligned}
\widetilde{\boldsymbol{\mathcal{J}}}_K^{(1)}(\mathbf{U}_h) &= -\frac{1}{2|K|}\sum_{\mathscr{E}\in\partial K}\left[|\mathscr{E}|\Big(\langle \mathbf{n}_{\mathscr{E},K}, \mathbf{F}(\bar{\mathbf{U}}_K) + \mathbf{F}(\bar{\mathbf{U}}_{K_{\mathscr{E}}})\rangle - a(\bar{\mathbf{U}}_{K_{\mathscr{E}}} - \bar{\mathbf{U}}_K)\Big)\right] \\
&= -\frac{1}{2|K|}\sum_{\mathscr{E}\in\partial K}\left[|\mathscr{E}|\Big(\langle \mathbf{n}_{\mathscr{E},K}, \mathbf{F}(\bar{\mathbf{U}}_{K_{\mathscr{E}}})\rangle - a(\bar{\mathbf{U}}_{K_{\mathscr{E}}} - \bar{\mathbf{U}}_K)\Big)\right], \qquad (61) \\
\widetilde{\boldsymbol{\mathcal{J}}}_K^{(2)}(\mathbf{U}_h) &= -\frac{1}{2|K|}\sum_{\mathscr{E}\in\partial K}\Big(|\mathscr{E}|\,\langle \mathbf{n}_{\mathscr{E},K}, \bar{\mathbf{B}}_{K_{\mathscr{E}}} - \bar{\mathbf{B}}_K\rangle\,\mathbf{S}\left(\bar{\mathbf{U}}_K\right)\Big) \\
&= -\frac{1}{2|K|}\sum_{\mathscr{E}\in\partial K}\Big(|\mathscr{E}|\,\langle \mathbf{n}_{\mathscr{E},K}, \bar{\mathbf{B}}_{K_{\mathscr{E}}}\rangle\,\mathbf{S}\left(\bar{\mathbf{U}}_K\right)\Big), \qquad (62)
\end{aligned}$$

where the identity $\sum_{\mathscr{E}\in\partial K}|\mathscr{E}|\mathbf{n}_{\mathscr{E},K}=\mathbf{0}$ has been used. In order to prove the PCP property (31), it suffices to show

$$\bar{\mathbf{U}}_K^{\Delta t}:=\bar{\mathbf{U}}_K+\Delta t\widetilde{\boldsymbol{\mathcal{J}}}_K(\mathbf{U}_h)\in\mathcal{G},\qquad\forall K\in\mathcal{T}_h, \tag{63}$$

under the CFL type condition (52) and the condition that $\bar{\mathbf{U}}_K\in\mathcal{G},\ \forall K\in\mathcal{T}_h$. In the following, we prove (63) by using the second equivalent form $\mathcal{G}_2=\mathcal{G}$ in Lemma 3.2 and verifying that $\bar{\mathbf{U}}_K^{\Delta t}\in\mathcal{G}_2,\ \forall K\in\mathcal{T}_h$.

We first show that the mass density $\bar{D}_K^{\Delta t}>0$. Recalling that the first component of $\mathbf{S}(\mathbf{U})$ is zero, we know that the first component of $\widetilde{\mathcal{J}}_K^{(2)}$ is zero. Then, we obtain

$$\begin{aligned}\bar{D}_K^{\Delta t}&=\bar{D}_K-\frac{\Delta t}{2|K|}\sum_{\mathscr{E}\in\partial K}\left[|\mathscr{E}|\Big(\bar{D}_{K_{\mathscr{E}}}\langle\mathbf{n}_{\mathscr{E},K},\bar{\mathbf{v}}_{K_{\mathscr{E}}}\rangle-a(\bar{D}_{K_{\mathscr{E}}}-\bar{D}_K)\Big)\right]\\&=\left(1-\frac{a\Delta t}{2|K|}\sum_{\mathscr{E}\in\partial K}|\mathscr{E}|\right)\bar{D}_K+\frac{\Delta t}{2|K|}\sum_{\mathscr{E}\in\partial K}\left[|\mathscr{E}|\left(a-\langle\mathbf{n}_{\mathscr{E},K},\bar{\mathbf{v}}_{K_{\mathscr{E}}}\rangle\right)\bar{D}_{K_{\mathscr{E}}}\right]\geq 0,\end{aligned}$$

where we have used the CFL condition (52) and $\langle\mathbf{n}_{\mathscr{E},K},\bar{\mathbf{v}}_{K_{\mathscr{E}}}\rangle\leq|\bar{\mathbf{v}}_{K_{\mathscr{E}}}|<1=c=a$.

We then prove that $\bar{\mathbf{U}}_K^{\Delta t}\cdot\boldsymbol{\xi}^*+p_m^*>0$ for any auxiliary variables $\mathbf{B}^*\in\mathbb{R}^3$ and $\mathbf{v}^*\in\mathbb{B}_1(\mathbf{0})$, where $\boldsymbol{\xi}^*$ and p_m^* are functions of $(\mathbf{B}^*,\mathbf{v}^*)$ as defined in Lemma 3.2. Using the inequality (23) in Lemma 3.6 gives

$$\left(\bar{\mathbf{U}}_{K_{\mathscr{E}}}-\frac{1}{a}\big\langle\mathbf{n}_{\mathscr{E},K},\mathbf{F}(\bar{\mathbf{U}}_{K_{\mathscr{E}}})\big\rangle\right)\cdot\boldsymbol{\xi}^*+p_m^*\geq\frac{1}{a}\left(\langle\mathbf{n}_{\mathscr{E},K},\mathbf{v}^*\rangle p_m^*-\langle\mathbf{n}_{\mathscr{E},K},\bar{\mathbf{B}}_{K_{\mathscr{E}}}\rangle(\mathbf{v}^*\cdot\mathbf{B}^*)\right).$$

It, along with (61), imply that

$$\begin{aligned}\widetilde{\boldsymbol{\mathcal{J}}}_K^{(1)}(\mathbf{U}_h)\cdot\boldsymbol{\xi}^*&=-\frac{a}{2|K|}\sum_{\mathscr{E}\in\partial K}\left[|\mathscr{E}|\left(\bar{\mathbf{U}}_K\cdot\boldsymbol{\xi}^*+p_m^*\right)\right]\\&\quad+\frac{a}{2|K|}\sum_{\mathscr{E}\in\partial K}\left\{|\mathscr{E}|\left[\left(\bar{\mathbf{U}}_{K_{\mathscr{E}}}-\frac{1}{a}\big\langle\mathbf{n}_{\mathscr{E},K},\mathbf{F}(\bar{\mathbf{U}}_{K_{\mathscr{E}}})\big\rangle\right)\cdot\boldsymbol{\xi}^*+p_m^*\right]\right\}\\&\geq-\frac{a}{2|K|}\sum_{\mathscr{E}\in\partial K}\left[|\mathscr{E}|\left(\bar{\mathbf{U}}_K\cdot\boldsymbol{\xi}^*+p_m^*\right)\right]\\&\quad+\frac{1}{2|K|}\sum_{\mathscr{E}\in\partial K}\left\{|\mathscr{E}|\Big[\langle\mathbf{n}_{\mathscr{E},K},\mathbf{v}^*\rangle p_m^*-\langle\mathbf{n}_{\mathscr{E},K},\bar{\mathbf{B}}_{K_{\mathscr{E}}}\rangle(\mathbf{v}^*\cdot\mathbf{B}^*)\Big]\right\}\\&=-\frac{a}{2|K|}\sum_{\mathscr{E}\in\partial K}\left(|\mathscr{E}|\left(\bar{\mathbf{U}}_K\cdot\boldsymbol{\xi}^*+p_m^*\right)\right)-\frac{\mathbf{v}^*\cdot\mathbf{B}^*}{2|K|}\sum_{\mathscr{E}\in\partial K}|\mathscr{E}|\langle\mathbf{n}_{\mathscr{E},K},\bar{\mathbf{B}}_{K_{\mathscr{E}}}\rangle,\end{aligned}$$

where the identity $\sum_{\mathscr{E}\in\partial K}|\mathscr{E}|\mathbf{n}_{\mathscr{E},K}=\mathbf{0}$ has been used in the last equality. Combining (62) and

the above estimate, we obtain

$$\begin{aligned}
\bar{\mathbf{U}}_K^{\Delta t}\cdot\boldsymbol{\xi}^*+p_m^* &= \bar{\mathbf{U}}_K\cdot\boldsymbol{\xi}^*+p_m^*+\Delta t\widetilde{\boldsymbol{\mathcal{J}}}_K^{(1)}(\mathbf{U}_h)\cdot\boldsymbol{\xi}^*+\Delta t\widetilde{\boldsymbol{\mathcal{J}}}_K^{(2)}(\mathbf{U}_h)\cdot\boldsymbol{\xi}^*\\
&\geq \bar{\mathbf{U}}_K\cdot\boldsymbol{\xi}^*+p_m^*-\frac{a\Delta t}{2|K|}\sum_{\mathscr{E}\in\partial K}|\mathscr{E}|\left(\bar{\mathbf{U}}_K\cdot\boldsymbol{\xi}^*+p_m^*\right)\\
&\quad-\frac{\Delta t}{2|K|}\sum_{\mathscr{E}\in\partial K}|\mathscr{E}|\langle\mathbf{n}_{\mathscr{E},K},\bar{\mathbf{B}}_{K_{\mathscr{E}}}\rangle\left(\mathbf{S}\left(\bar{\mathbf{U}}_K\right)\cdot\boldsymbol{\xi}^*+\mathbf{v}^*\cdot\mathbf{B}^*\right)\\
&\geq \left(1-\frac{a\Delta t}{2|K|}\sum_{\mathscr{E}\in\partial K}|\mathscr{E}|\right)\left(\bar{\mathbf{U}}_K\cdot\boldsymbol{\xi}^*+p_m^*\right)\\
&\quad-\frac{\Delta t}{2|K|}\left|\sum_{\mathscr{E}\in\partial K}|\mathscr{E}|\langle\mathbf{n}_{\mathscr{E},K},\bar{\mathbf{B}}_{K_{\mathscr{E}}}\rangle\right|\left|\mathbf{S}\left(\bar{\mathbf{U}}_K\right)\cdot\boldsymbol{\xi}^*+\mathbf{v}^*\cdot\mathbf{B}^*\right|.
\end{aligned}$$

Thanks to Lemma 3.4, we obtain

$$\begin{aligned}
\bar{\mathbf{U}}_K^{\Delta t}\cdot\boldsymbol{\xi}^*+p_m^* &\geq \left(1-\frac{a\Delta t}{2|K|}\sum_{\mathscr{E}\in\partial K}|\mathscr{E}|\right)\left(\bar{\mathbf{U}}_K\cdot\boldsymbol{\xi}^*+p_m^*\right)\\
&\quad-\frac{\Delta t}{2|K|}\left|\sum_{\mathscr{E}\in\partial K}|\mathscr{E}|\langle\mathbf{n}_{\mathscr{E},K},\bar{\mathbf{B}}_{K_{\mathscr{E}}}\rangle\right|\frac{1}{\sqrt{\bar{\rho}_K\bar{H}_K}}\left(\bar{\mathbf{U}}_K\cdot\boldsymbol{\xi}^*+p_m^*\right)\\
&= \left(1-\frac{a\Delta t}{2|K|}\sum_{\mathscr{E}\in\partial K}\left|\mathscr{E}\right|-\Delta t\frac{|\mathrm{div}_K\mathbf{B}_h|}{\sqrt{\bar{\rho}_K\bar{H}_K}}\right)\left(\bar{\mathbf{U}}_K\cdot\boldsymbol{\xi}^*+p_m^*\right)>0,
\end{aligned}$$

where the identity $\sum_{\mathscr{E}\in\partial K}|\mathscr{E}|\mathbf{n}_{\mathscr{E},K}=\mathbf{0}$ has been used in the equality, and the CFL condition (52) is used in the last inequality. Therefore, we have

$$\bar{\mathbf{U}}_K^{\Delta t}\cdot\boldsymbol{\xi}^*+p_m^*>0,\qquad\forall\mathbf{B}^*\in\mathbb{R}^3,\quad\forall\mathbf{v}^*\in\mathbb{B}_1(\mathbf{0}),$$

which, along with $\bar{D}_K^{\Delta t}>0$, yield $\bar{\mathbf{U}}_K^{\Delta t}\in\mathcal{G}_2=\mathcal{G}$. The proof is complete.

References

[1] D. S. Balsara, *Second-order-accurate schemes for magnetohydrodynamics with divergence-free reconstruction*, Astrophys. J. Suppl. Ser., 151 (2004), pp. 149–184.

[2] D. S. Balsara and J. Kim, *A subluminal relativistic magnetohydrodynamics scheme with ADER-WENO predictor and multidimensional Riemann solver-based corrector*, J. Comput. Phys., 312 (2016), pp. 357–384.

[3] D. S. Balsara and D. Spicer, *A staggered mesh algorithm using high order Godunov fluxes to ensure solenoidal magnetic fields in magnetohydrodynamic simulations*, J. Comput. Phys., 149 (1999), pp. 270–292.

[4] P. Chandrashekar, *A global divergence conforming DG method for hyperbolic conservation laws with divergence constraint*, J. Sci. Comput., 79 (2019), pp. 79–102.

[5] A. J. Christlieb, Y. Liu, Q. Tang, and Z. Xu, *Positivity-preserving finite difference weighted ENO schemes with constrained transport for ideal magnetohydrodynamic equations*, SIAM J. Sci. Comput., 37 (2015), pp. A1825–A1845.

[6] B. Cockburn, S. Hou, and C.-W. Shu, *The Runge-Kutta local projection discontinuous Galerkin finite element method for conservation laws. IV. The multidimensional case*, Math. Comp., 54 (1990), pp. 545–581.

[7] B. Cockburn, F. Li, and C.-W. Shu, *Locally divergence-free discontinuous Galerkin methods for the Maxwell equations*, J. Comput. Phys., 194 (2004), pp. 588–610.

[8] B. Cockburn and C.-W. Shu, *TVB Runge-Kutta local projection discontinuous Galerkin finite element method for conservation laws. II. General framework*, Math. Comp., 52 (1989), pp. 411–435.

[9] A. Dedner, F. Kemm, D. Kröner, C.-D. Munz, T. Schnitzer, and M. Wesenberg, *Hyperbolic divergence cleaning for the MHD equations*, J. Comput. Phys., 175 (2002), pp. 645–673.

[10] L. Del Zanna, O. Zanotti, N. Bucciantini, and P. Londrillo, *ECHO: a Eulerian conservative high-order scheme for general relativistic magnetohydrodynamics and magnetodynamics*, Astron. & Astrophys., 473 (2007), pp. 11–30.

[11] J. Du and C.-W. Shu, *Positivity-preserving high-order schemes for conservation laws on arbitrarily distributed point clouds with a simple WENO limiter*, Int. J. Numer. Anal. Model., 15 (2018), pp. 1–25.

[12] C. R. Evans and J. F. Hawley, *Simulation of magnetohydrodynamic flows: a constrained transport method*, Astrophys. J., 332 (1988), pp. 659–677.

[13] P. Fu, F. Li, and Y. Xu, *Globally divergence-free discontinuous Galerkin methods for ideal magnetohydrodynamic equations*, J. Sci. Comput., 77 (2018), pp. 1621–1659.

[14] S. K. Godunov, *Symmetric form of the equations of magnetohydrodynamics*, Numerical Methods for Mechanics of Continuum Medium, 1 (1972), pp. 26–34.

[15] S. Gottlieb, C.-W. Shu, and E. Tadmor, *Strong stability-preserving high-order time discretization methods*, SIAM Rev., 43 (2001), pp. 89–112.

[16] J.-L. Guermond, M. Nazarov, B. Popov, and I. Tomas, *Second-order invariant domain preserving approximation of the Euler equations using convex limiting*, SIAM J. Sci. Comput., 40 (2018), pp. A3211–A3239.

[17] P. He and H. Tang, *An adaptive moving mesh method for two-dimensional relativistic magnetohydrodynamics*, Comput. Fluids, 60 (2012), pp. 1–20.

[18] X. Y. Hu, N. A. Adams, and C.-W. Shu, *Positivity-preserving method for high-order conservative schemes solving compressible Euler equations*, J. Comput. Phys., 242 (2013), pp. 169–180.

[19] Y. Jiang and H. Liu, *Invariant-region-preserving DG methods for multi-dimensional hyperbolic conservation law systems, with an application to compressible Euler equations*, J. Comput. Phys., 373 (2018), pp. 385–409.

[20] S. S. Komissarov, *A Godunov-type scheme for relativistic magnetohydrodynamics*, Mon. Not. R. Astron. Soc., 303 (1999), pp. 343–366.

[21] L. Krivodonova, J. Xin, J.-F. Remacle, N. Chevaugeon, and J. E. Flaherty, *Shock detection and limiting with discontinuous Galerkin methods for hyperbolic conservation laws*, Appl. Numer. Math., 48 (2004), pp. 323–338.

[22] F. Li and C.-W. Shu, *Locally divergence-free discontinuous Galerkin methods for MHD equations*, J. Sci. Comput., 22 (2005), pp. 413–442.

[23] F. Li, L. Xu, and S. Yakovlev, *Central discontinuous Galerkin methods for ideal MHD equations with the exactly divergence-free magnetic field*, J. Comput. Phys., 230 (2011), pp. 4828–4847.

[24] C. Liang and Z. Xu, *Parametrized maximum principle preserving flux limiters for high order schemes solving multi-dimensional scalar hyperbolic conservation laws*, J. Sci. Comput., 58 (2014), pp. 41–60.

[25] D. Ling, J. Duan, and H. Tang, *Physical-constraints-preserving Lagrangian finite volume schemes for one- and two-dimensional special relativistic hydrodynamics*, J. Comput. Phys., 396 (2019), pp. 507–543.

[26] A. Mignone and G. Bodo, *An HLLC riemann solver for relativistic flows–II. magnetohydrodynamics*, Mon. Not. R. Astron. Soc., 368 (2006), pp. 1040–1054.

[27] S. Mishra and E. Tadmor, *Constraint preserving schemes using potential-based fluxes. III. Genuinely multi-dimensional schemes for MHD equations*, ESAIM: Mathematical Modelling and Numerical Analysis, 46 (2012), pp. 661–680.

[28] K. G. Powell, *An approximate Riemann solver for magnetohydrodynamics (that works in more than one dimension)*, Tech. Report ICASE Report No. 94-24, NASA Langley, VA, 1994.

[29] K. G. Powell, P. L. Roe, T. J. Linde, T. I. Gombosi, and D. L. D. Zeeuw, *A solution-adaptive upwind scheme for ideal magnetohydrodynamics*, J. Comput. Phys., 154 (1999), pp. 284 – 309.

[30] T. Qin, C.-W. Shu, and Y. Yang, *Bound-preserving discontinuous Galerkin methods for relativistic hydrodynamics*, J. Comput. Phys., 315 (2016), pp. 323–347.

[31] J. Qiu and C.-W. Shu, *Runge–Kutta discontinuous Galerkin method using WENO limiters*, SIAM J. Sci. Comput., 26 (2005), pp. 907–929.

[32] D. Radice, L. Rezzolla, and F. Galeazzi, *High-order fully general-relativistic hydrodynamics: new approaches and tests*, Classical and Quantum Gravity, 31 (2014), p. 075012.

[33] C.-W. Shu, *Bound-preserving high-order schemes for hyperbolic equations: Survey and recent developments*, in Theory, Numerics and Applications of Hyperbolic Problems II, C. Klingenberg and M. Westdickenberg, eds., Cham, 2018, Springer International Publishing, pp. 591–603.

[34] Z. Sun and C.-w. Shu, *Strong stability of explicit Runge–Kutta time discretizations*, SIAM J. Numer. Anal., 57 (2019), pp. 1158–1182.

[35] E. Tadmor, *A minimum entropy principle in the gas dynamics equations*, Applied Numerical Mathematics, 2 (1986), pp. 211–219.

[36] M. Torrilhon, *Locally divergence-preserving upwind finite volume schemes for magnetohydrodynamic equations*, SIAM J. Sci. Comput., 26 (2005), pp. 1166–1191.

[37] G. Tóth, *The $\nabla \cdot \mathbf{B} = 0$ constraint in shock-capturing magnetohydrodynamics codes*, J. Comput. Phys., 161 (2000), pp. 605–652.

[38] B. van der Holst, R. Keppens, and Z. Meliani, *A multidimensional grid-adaptive relativistic magnetofluid code*, Comput. Phys. Commun., 179 (2008), pp. 617–627.

[39] K. Wu, *Design of provably physical-constraint-preserving methods for general relativistic hydrodynamics*, Phys. Rev. D, 95 (2017), 103001.

[40] K. Wu, *Positivity-preserving analysis of numerical schemes for ideal magnetohydrodynamics*, SIAM J. Numer. Anal., 56 (2018), pp. 2124–2147.

[41] K. Wu, *Minimum principle on specific entropy and high-order accurate invariant region preserving numerical methods for relativistic hydrodynamics*, arXiv preprint arXiv:2102.03801, (2021).

[42] K. Wu and C.-W. Shu, *A provably positive discontinuous Galerkin method for multidimensional ideal magnetohydrodynamics*, SIAM J. Sci. Comput., 40 (2018), pp. B1302–B1329.

[43] K. Wu and C.-W. Shu, *Provably positive high-order schemes for ideal magnetohydrodynamics: analysis on general meshes*, Numer. Math., 142 (2019), pp. 995–1047.

[44] K. Wu and C.-W. Shu, *Entropy symmetrization and high-order accurate entropy stable numerical schemes for relativistic MHD equations*, SIAM J. Sci. Comput., 42 (2020), pp. A2230–A2261.

[45] K. Wu and H. Tang, *High-order accurate physical-constraints-preserving finite difference WENO schemes for special relativistic hydrodynamics*, J. Comput. Phys., 298 (2015), pp. 539–564.

[46] K. Wu and H. Tang, *Admissible states and physical-constraints-preserving schemes for relativistic magnetohydrodynamic equations*, Math. Models Methods Appl. Sci., 27 (2017), pp. 1871–1928.

[47] K. Wu and H. Tang, *Physical-constraint-preserving central discontinuous Galerkin methods for special relativistic hydrodynamics with a general equation of state*, Astrophys. J. Suppl. Ser., 228 (2017), 3.

[48] K. Wu and H. Tang, *On physical-constraints-preserving schemes for special relativistic magnetohydrodynamics with a general equation of state*, Z. Angew. Math. Phys., 69 (2018), 84.

[49] Z. Xu, *Parametrized maximum principle preserving flux limiters for high order schemes solving hyperbolic conservation laws: one-dimensional scalar problem*, Math. Comp., 83 (2014), pp. 2213–2238.

[50] Z. Xu and Y. Liu, *New central and central discontinuous Galerkin schemes on overlapping cells of unstructured grids for solving ideal magnetohydrodynamic equations with globally divergence-free magnetic field*, J. Comput. Phys., 327 (2016), pp. 203–224.

[51] O. Zanotti, F. Fambri, and M. Dumbser, *Solving the relativistic magnetohydrodynamics equations with ADER discontinuous Galerkin methods, a posteriori subcell limiting and adaptive mesh refinement*, Mon. Not. R. Astron. Soc., 452 (2015), pp. 3010–3029.

[52] X. Zhang, *On positivity-preserving high order discontinuous Galerkin schemes for compressible Navier-Stokes equations*, J. Comput. Phys., 328 (2017), pp. 301–343.

[53] X. Zhang and C.-W. Shu, *On maximum-principle-satisfying high order schemes for scalar conservation laws*, J. Comput. Phys., 229 (2010), pp. 3091–3120.

[54] X. Zhang and C.-W. Shu, *On positivity-preserving high order discontinuous Galerkin schemes for compressible Euler equations on rectangular meshes*, J. Comput. Phys., 229 (2010), pp. 8918–8934.

[55] X. Zhang and C.-W. Shu, *A minimum entropy principle of high order schemes for gas dynamics equations*, Numer. Math., 121 (2012), pp. 545–563.

[56] X. Zhang, Y. Xia, and C.-W. Shu, *Maximum-principle-satisfying and positivity-preserving high order discontinuous Galerkin schemes for conservation laws on triangular meshes*, J. Sci. Comput., 50 (2012), pp. 29–62.

[57] J. Zhao and H. Tang, *Runge-Kutta discontinuous Galerkin methods for the special relativistic magnetohydrodynamics*, J. Comput. Phys., 343 (2017), pp. 33–72.

[58] S. Zou, X. Yu, and Z. Dai, *A positivity-preserving Lagrangian discontinuous Galerkin method for ideal magnetohydrodynamics equations in one-dimension*, J. Comput. Phys., 405 (2020), p. 109144.